Rev Environ Sci Biotechnol (2023) 22:55–78
https://doi.org/10.1007/s11157-023-09646-3

REVIEW PAPER

# Aqueous Fe(II)-catalyzed iron oxide recrystallization: Fe redox cycling and atom exchange, mineralogical recrystallization and contributing factor

**Jian Hua · Jing Sun · Manjia Chen · Chengshuai Liu · Feng Wu**

Received: 25 September 2022 / Accepted: 28 January 2023 / Published online: 14 February 2023


**Abstract** Iron (Fe) oxides can rapidly recrystallize in the presence of aqueous Fe(II) ($Fe(II)_{aq}$) under anoxic conditions. Since different Fe oxides have diverse affinities and redox reactivities for metal(loid)s, nutrients, and organic matters, recrystallization of Fe oxides significantly alters their speciation and environmental behavior. Therefore, the major reaction steps, rates, and influencing factors of $Fe(II)_{aq}$-catalyzed recrystallization have gained increasing attention. This paper aims to review the latest advances, especially in redox cycling between $Fe(II)_{aq}$ and Fe oxide and in the kinetics of Fe atom exchange. The mineralogical recrystallization pathways and intermediate processes of different Fe oxides when exposed to $Fe(II)_{aq}$ are discussed. The influencing factors such as morphological natures of Fe oxides and typical environmental substances governing the kinetics of isotopic exchange between $Fe(II)_{aq}$ and Fe oxides are summarized. Several major analytical methodologies in this realm are also illustrated. Finally, some unsolved issues and future research directions in the field of $Fe(II)_{aq}$-catalyzed Fe oxide recrystallization are outlined.

J. Hua · F. Wu
School of Resources and Environmental Science, Wuhan University, Wuhan 430079, China

J. Hua · J. Sun (✉) · C. Liu (✉)
State Key Laboratory of Environmental Geochemistry, Institute of Geochemistry, Chinese Academy of Sciences, Guiyang 550081, China
e-mail: sunjing@mail.gyig.ac.cn

C. Liu
e-mail: liuchengshuai@vip.gyig.ac.cn

M. Chen · C. Liu
National-Regional Joint Engineering Research Center for Soil Pollution Control and Remediation in South China, Guangdong Key Laboratory of Integrated Agro-Environmental Pollution Control and Management, Institute of Eco Environmental and Soil Sciences, Guangdong Academy of Sciences, Guangzhou 510650, China

**Graphical abstract**

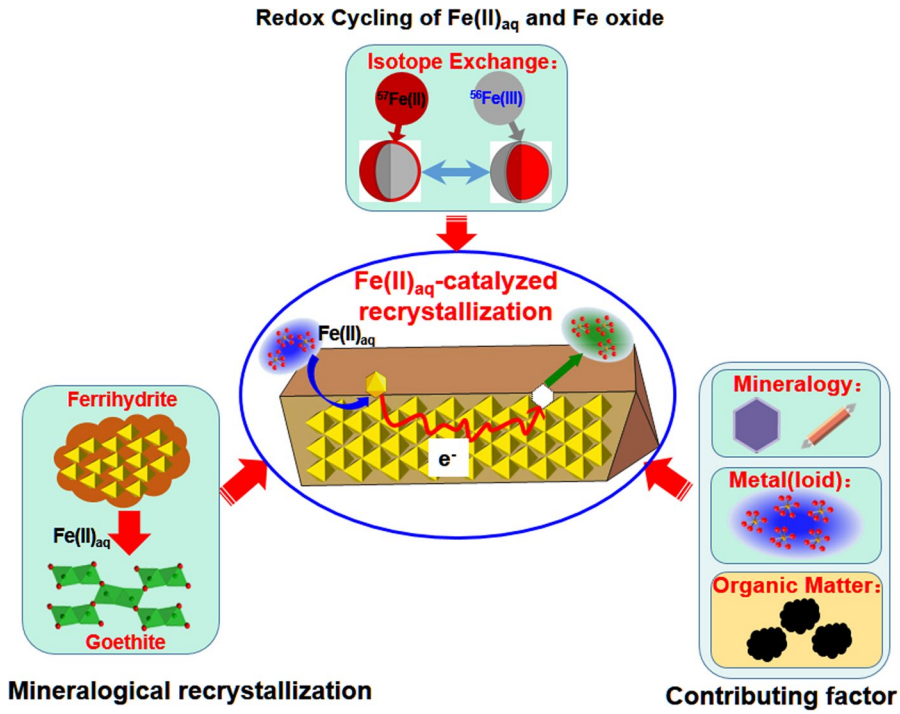


**Keywords** $Fe(II)_{aq}$-catalyzed recrystallization · Iron isotope tracer · Iron atom exchange · Phase transformation · Contributing factor

## 1 Introduction

Iron (Fe) is the most abundant redox-active metal on Earth, accounting for > 35% of the Earth's mass (Su and Liu 2019). Due to the presence of oxygen, Fe exists primarily as various ferric and mixed-valence Fe oxides, oxyhydroxides, and hydroxides (referred to hereafter as Fe oxides together) near the surface of the Earth's crust (Schwertmann et al. 1984; Stumm and Sulzberger 1992; Weber et al. 2006b). Fe oxides in soils can strongly influence the degradation and sequestration of organic carbon, the solubility and bioavailability of nutrients and inorganic contaminants, weathering and mineralization of rocks, and microbial activity (Eglinton 2012; Lalonde et al. 2012; Melton et al. 2014; Schwertmann 1983). Also, Fe oxides are frequently utilized for groundwater remediation by removing toxic or radioactive contaminants from groundwater through surface adsorption, surface precipitation and/or structural substitution (Cooper et al. 2000, 2006; Sun et al. 2016a, b).

In the absence of $Fe(II)_{aq}$, many Fe oxide minerals are thermodynamically stable under low temperatures of < 40 ℃ (Curti et al. 2010; Frierdich et al. 2015a; Hren et al. 2006; Schwertmann 1983; Schwertmann et al. 2004, 2005). In contrast, in the presence of $Fe(II)_{aq}$, Fe oxides can recrystallize within a few days at environmentally relevant pressure and temperatures (Gorski and Fantle 2017; Handler et al. 2014). The term "recrystallization" involves not only the transformation from one mineral phase to another but also the Fe oxide preserving its structure and chemical composition but changing its particle morphology (Joshi and Gorski 2016). These two phenomena both alter the effective reactivity of the Fe pool in the environments (Flynn and Catalano 2018; Lu et al. 2019; Zhou et al. 2018). Due to the ubiquitous coexistence of aqueous Fe(II) ($Fe(II)_{aq}$) and Fe oxides in soils and underground aquifers, $Fe(II)_{aq}$-catalyzed

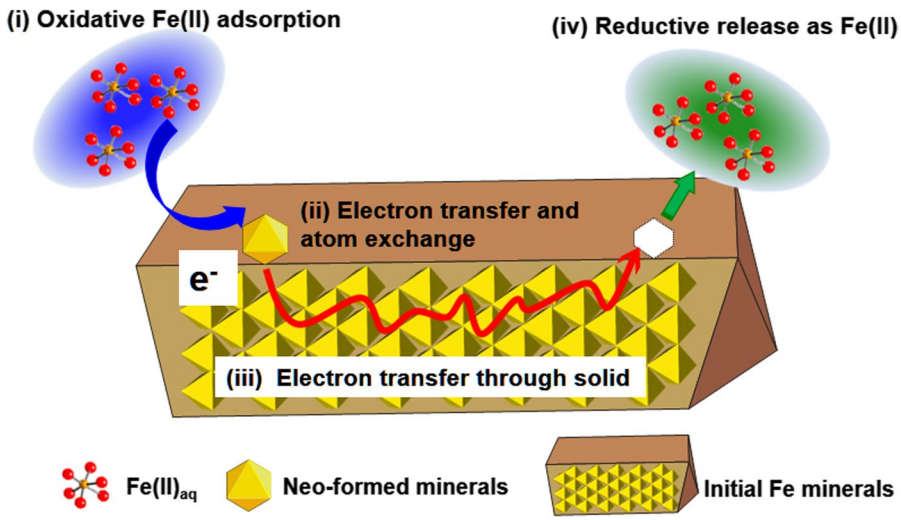


**Fig. 1** Schematic illustration of the hypothesized interfacial electron transfer between the adsorbed Fe(II) and surface/subsurface Fe(III) of Fe oxides, i.e., (1) oxidative Fe(II) adsorption, (2) electron transfer and atom exchange, (3) electron transfer through the solid, and (4) reductive release as Fe(II)

recrystallization of Fe oxides is a pervasive natural process (Brown et al. 1999; Stumm and Sulzberger 1992; Tishchenko et al. 2015). Numerous studies concerning different aspects of $Fe(II)_{aq}$-catalyzed recrystallization of Fe oxides have been conducted. Based on the findings, $Fe(II)_{aq}$-catalyzed Fe oxide recrystallization is now known to follow a multi-step mechanism (Fig. 1). Major steps involve (1) $Fe(II)_{aq}$ sorption, (2) electron and atom exchange between adsorbed Fe(II) and Fe(III) in Fe oxides, and (3) conduction of injected electrons to a distant Fe(III) lattice sites, which then undergo (4) reductive release as Fe(II) (Alexandrov and Rosso 2015; Handler et al. 2014). Redox cycling between $Fe(II)_{aq}$ and Fe(III) in Fe oxides is mechanically responsible for recrystallization of coupled growth (via sorption and electron transfer) and dissolution of Fe oxides (Alexandrov and Rosso 2015; Handler et al. 2014; Notini et al. 2019a). During recrystallization, Fe cycles from $Fe(II)_{aq}$ to adsorbed Fe(II) and then to a new Fe mineral phase, typically without changes in the abundance of Fe(II).

The extent of interfacial Fe atom exchange calculated by Fe isotopic tracer can be utilized to determine the degree of $Fe(II)_{aq}$-catalyzed Fe oxide recrystallization (Reddy et al. 2015). The kinetics of Fe atom exchange can be employed to assess the impacts of different factors on the rate of recrystallization, e.g., particle size of Fe oxide, $Fe(II)_{aq}$ concentration and pH condition (Frierdich et al. 2015b; Handler et al. 2014; Reddy et al. 2015). In addition, Fe isotopic tracer and spectroscopic techniques, e.g., $^{57}$Fe-Mössbauer spectroscopy and atom probe tomography (APT), can be used to determine Fe speciation and isotopic distribution in secondary minerals after exposed to $Fe(II)_{aq}$ (Larese-Casanova et al. 2012; Taylor et al. 2019b; Williams and Scherer 2004). These analytical methodologies provide new scope for probing the electron and atom exchange processes, thereby improving the understanding of the underlying mechanism of the interplay between Fe oxides and $Fe(II)_{aq}$.

In soils and underground aquifers, Fe oxides exhibit a strong affinity to environmental components such as metal(loid)s, organic matters (OMs), and microorganisms due to their high specific surface area and surface reactivity, which are mainly determined by their mineral phase, particle size, and surface defective extent (Chen et al. 2014; Cornell and Schwertmann 2004; Coward et al. 2018; Lu et al. 2020; Tessier et al. 1996). For instance, the initial Fe minerals can dominate the extents of atom exchange between $Fe(II)_{aq}$ and lattice Fe(III), e.g., 100% exchanges for ferrihydrite, 68% exchanges for goethite, and 10% exchanges for magnetite (Gorski et al. 2012; Reddy et al. 2015; ThomasArrigo et al. 2017). Furthermore, metal(loid)s such as aluminum (Al), zinc (Zn) and nickel (Ni), as well as OMs such as fulvic acids, can slow down the Fe atom exchange ratios, because both of them can block the reactive sites and prevent the dissolution of Fe oxides (Hu et al. 2020; Latta et al. 2012b; Liu et al. 2016; ThomasArrigo et al. 2017). In contrast, Fe(III)-reducing bacteria are able to promote recrystallization of Fe oxides by

accelerating Fe(II) production (Weber et al. 2006a; Xiao et al. 2018).

However, current investigations concerning $Fe(II)_{aq}$-catalyzed recrystallization have generated new issues. For instance, the formation of Fe(II) inner-sphere surface complex on Fe oxide is thought to be an essential step for the electron transfer during recrystallization (Alexandrov and Rosso 2015; Zarzycki et al. 2015a). Nonetheless, despite the shorter Fe(II)–Fe(III) atomic distances are more favorable for electron transfer (Kerisit et al. 2015), whether the formation of inner-sphere Fe(II) species is required to enable the electron transfer remains unclear. Moreover, using a rapid freeze–quench technique, a recent study detected the intermediate Fe(IV) species in Fe(II)-goethite suspensions (Hua et al. 2022). However, the use of in situ spectroscopic tools, such as in situ XAS and Mössbauer spectroscopy, to track the production of intermediate Fe species is currently rare. So far, most experimental studies focus on single Fe oxide coexisted with either metal(loid)s or OMs (Flynn and Catalano 2018; Frierdich and Catalano 2012; Kang et al. 2018; Karimian et al. 2019). It remains unclear how a variety of Fe minerals coexisting with multifarious environmental factors affect the recrystallization process.

Although abundant studies regarding $Fe(II)_{aq}$-catalyzed recrystallization have been conducted in the past decades, there is only a brief overview in this realm which focused on the incorporation and/or release of metal(loid)s (Latta et al. 2012b) and systematical reviews remain limited. In this review, major findings from the previous studies on $Fe(II)_{aq}$-catalyzed recrystallization are compiled and discussed. One of the focuses is to highlight the thermodynamics and kinetics of interfacial electron and atom exchange between $Fe(II)_{aq}$ and Fe(III) in Fe oxide. The mineralogical recrystallization of Fe oxides such as phase transformation and mineralogical changes are also illustrated. Moreover, the impacts of various contributing factors on the dynamics of interfacial isotopic exchange between Fe oxide and $Fe(II)_{aq}$ are summarized. Finally, unsolved issues and knowledge gaps that should be addressed in future research to advance the overall comprehension of the processes and mechanisms of $Fe(II)_{aq}$-catalyzed recrystallization are outlined.

## 2 Redox cycling of $Fe(II)_{aq}$ and Fe(III) during recrystallization

Owing to 20 years of research, the primary steps of electron and atom exchange during $Fe(II)_{aq}$-catalyzed recrystallization have been discovered (Fig. 1). The protonation or deprotonation of hydroxyl groups invokes a charge on the mineral surface, which is responsible for the surface affinity of Fe oxides to Fe(II) and many other ions (Hiemstra and Riemsdijk 1999; Hiemstra et al. 1996). Once the distances between Fe(II) and crystal surface reduce to 1–1.5 Å, the inner-sphere complex at the mineral surface can form (Zarzycki et al. 2015a). The Fe(II) inner-sphere surface complex on Fe oxide initiates the interfacial electron transfer via electronic donor–acceptor coupling (Alexandrov and Rosso 2014; Zarzycki et al. 2015a). The donated electron shuttles along the Fe chains in directions parallel to the facet of Fe oxides, which requires less energy than conduction through a resistant mineral bulk (Zarzycki et al. 2015a). The subsequently generated labile Fe intermediates assemble into the nuclei of neoformed mineral products through the olation and oxolation reactions, in a manner that coincides with Classical Nucleation Theory (Sheng et al. 2020a, b). To summarize the recent findings on redox cycling between $Fe(II)_{aq}$ and Fe(III) during $Fe(II)_{aq}$-catalyzed recrystallization, here we discuss (1) the redox equilibrium between $Fe(II)_{aq}$ and Fe oxides, (2) the interfacial Fe(II)–Fe(III) atom exchanges, and (3) the isotopic exchange models.

### 2.1 Redox equilibrium of $Fe(II)_{aq}$ and Fe oxides

The accumulation of Fe(II) on Fe oxide surface, the first step to initiate the interfacial Fe(II)–Fe(III) interaction, controls the thermodynamic driving force of $Fe(II)_{aq}$-catalyzed recrystallization (Alexandrov and Rosso 2015; Frierdich et al. 2015b). To disclose whether Fe(II) adsorbed on Fe oxides is more prone to be oxidized than $Fe(II)_{aq}$, the reduction potential ($E_H$) of solid-adsorbed Fe(II) was compared with that of $Fe(II)_{aq}$ by Gorski et al. (2016). The results showed that $Fe(II)_{aq}$ and solid-adsorbed Fe(II) have same $E_H$ value and can reach redox equilibrium with each other (Gorski et al. 2016). However, during $Fe(II)_{aq}$-catalyzed recrystallization, the coexisted Fe oxide phases can affect the $E_H$ value of adsorbed Fe(II) through

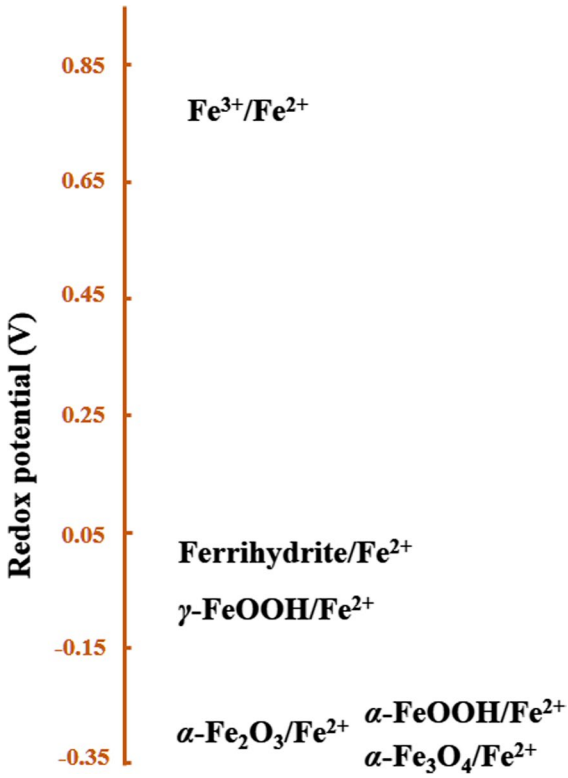


**Fig. 2** The redox potentials of various Fe(III)/Fe(II) couples (temperature = 25 °C, pH 7, $[Fe^{2+}] = 10$ μM). The figure is reproduced from the data in Thamdrup (2000), with permission from Springer publications

forming different oxidation products (Catalano et al. 2010; Felmy et al. 2011; Schwertmann et al. 1984).

The reduction potentials for redox couples of Fe(II) and diverse Fe oxides are shown in Fig. 2 (Liu et al. 2022; Thamdrup 2000). The standard reduction potential ($E^0_H$) value of a redox couple of $Fe(II)_{aq}$ and a crystalline Fe oxide phase is lower than $E^0_H$ value of $Fe(II)_{aq}$ and aqueous Fe(III) under comparable conditions (Gorski et al. 2016). The $E_H$ of Fe(II)-ferrihydrite suspension quickly decreases in accompany with the production of lepidocrocite and goethite (Boland et al. 2013; Jones et al. 2017). The decrease in $E_H$ value with recrystallization to goethite supports that the reductive capacity of Fe(II) is enhanced when associated with goethite compared to that with ferrihydrite. In addition, while in the absence of Fe oxides, the oxidation of $Fe(II)_{aq}$ can only form aqueous Fe(III) or amorphous ferrihydrite (Schwertmann et al. 1984). When a Fe oxide such as ferrihydrite is present, diverse crystalline Fe oxide phases including lepidocrocite and goethite can form (Chun et al. 2006; Larese-Casanova et al. 2012; Schwertmann et al. 1984). Fe oxides with high crystallinity have more negative Gibbs free energy than ferrihydrite (Gorski et al. 2016). Therefore, the solid-adsorbed Fe(II) in the presence of Fe oxide phases are favorable for electron injection into the surficial Fe lattice, further initialing the recrystallization of Fe oxide.

### 2.2 Interfacial Fe(II)–Fe(III) atom exchanges

Exchanges of Fe atom between $Fe(II)_{aq}$ and Fe oxides can be used to identify the recrystallization of coupled growth and dissolution of Fe oxides (Handler et al. 2009; Williams and Scherer 2004). By tracing the changes in Fe isotope distribution across aqueous and solid phases, the interfacial Fe(II)–Fe(III) atom exchange were determined in the literatures (Frierdich et al. 2012; ThomasArrigo et al. 2017). For instance, when $^{55}$Fe-labelled Fe oxides interact with natural $Fe(II)_{aq}$ under anoxic conditions, an apparent release of $^{55}$Fe from the isotope-labelled Fe oxides is observed (Pedersen et al. 2005). In addition, an tendency of isotope equilibrium between $Fe(II)_{aq}$ and Fe oxides with diverse initial $\delta^{57/56}$Fe values ($\delta^{57/56}$Fe refer to the $^{57}$Fe/$^{56}$Fe proportion relative to the IRMM-014 isotope standard) is observed during recrystallization (Handler et al. 2009). Isotope tracers can be used in combination with APT to disclose the non-uniform Fe isotopic distribution in Fe mineral grain in three dimensions. Using this technique, Frierdich et al. (2019b) and Taylor et al. (2019b) indicated that the concentration of injected $^{57}$Fe was the highest near the grain periphery and then decreased with depth (Fig. 3). Moreover, the interfacial Fe isotope exchange between $^{57}Fe(II)_{aq}$ and $^{56}$Fe(III) in Fe oxides can be characterized using $^{57}$Fe Mössbauer spectroscopy, resulting from the formation of $^{57}$Fe-minerals in the secondary minerals (Williams and Scherer 2004).

Beside Fe, structural oxygen in Fe oxides can also undergo atom exchange with the oxygen in water molecules (Frierdich et al. 2015a; Jakub et al. 2021). However, when ~ 60% of Fe atom exchange occurs during $Fe(II)_{aq}$-catalyzed recrystallization, only ~ 20% of the oxygen in goethite is exchanged simultaneously

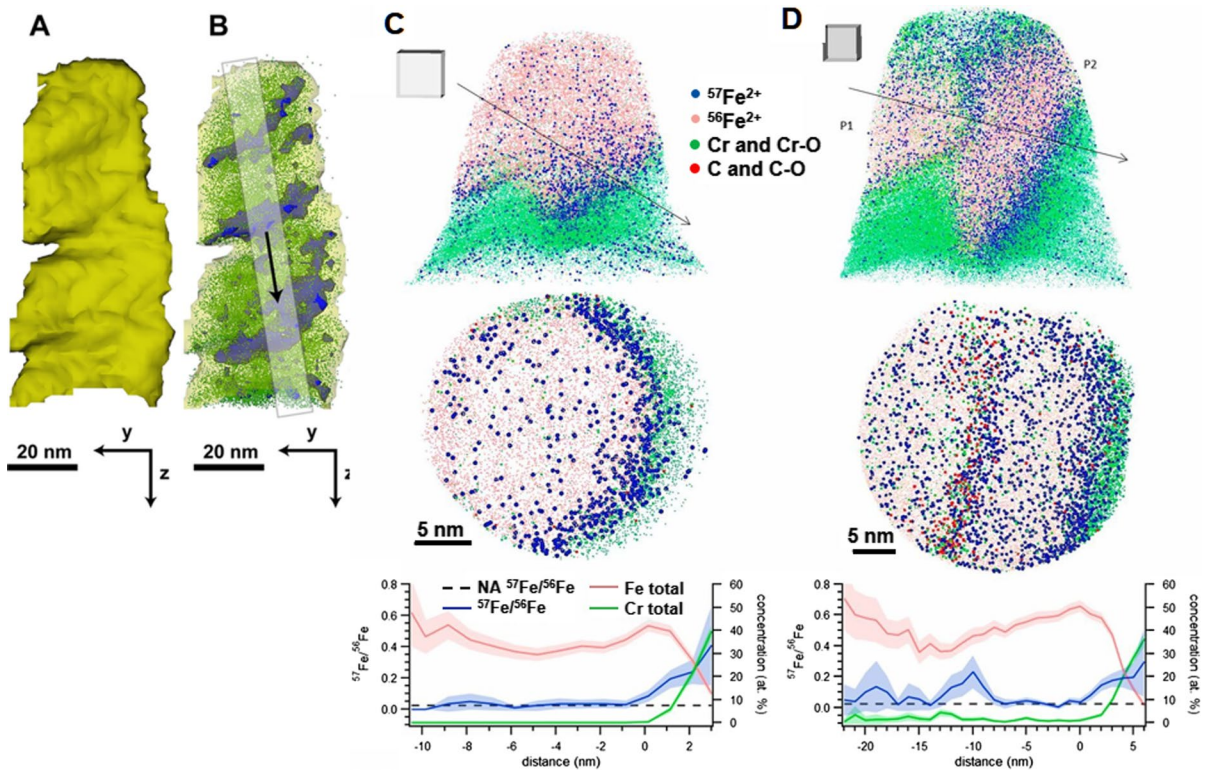


**Fig. 3** **a** Reconstruction of grain boundaries of goethite reacted with $^{57}$Fe-enriched Fe(II)$_{aq}$ for 30 days. **b** Distribution of $^{56}$Fe (green dots) and goethite regions with particularly high enrichments of $^{57}$Fe (blue region). This figure is adopted from Frierdich et al. (2019a, b). Copyright 2019, with permission from ACS Publications. APT reconstructions of goethite grain at two different locations (referred to as (**c**) and (**d**)), where **c** exhibits 57Fe enrichment at the exterior surfaces and **d** highlights intergranular diffusion of 57Fe. The 57Fe/56Fe values correspond to the y axis on the left-hand side, while the Cr and Fe concentrations correspond to the y axis on the right-hand side. The onset of the goethite phase is set to 0 nm, and the vertical, gray dashed lines mark the onset of the nominally nonrecrystallized phase, i.e., where 57Fe/56Fe reaches natural abundance (referred to NA). Solid arrows through full tip reconstructions indicate the ~2-nm-thick region for cross-section measurements; 5-nm cubes are used for scale. Data from Taylor et al. (2019a, b). Copyright (2019) National Academy of Sciences

(Frierdich et al. 2015a). The different oxygen sites in goethite may result in the different exchange extents between O and Fe atom in same system. The goethite surface contains a variety of oxygen sites, including singly-coordinated water molecules, doubly-coordinated hydroxyl groups, and triply-coordinated hydroxyl and oxo groups (Balogh et al. 2007). During Fe(II)$_{aq}$-catalyzed recrystallization, the singly coordinated water molecules on goethite are in oxygen isotope equilibrium with the solution already, but can still undergo isotopic exchange with water. The doubly and triply coordinated surface oxygen groups on goethite, on the other hand, may not interact with the solution (Balogh et al. 2007; Frierdich et al. 2015a). Therefore, less O atom exchanges relative to Fe atom are observed (Frierdich et al. 2015a).

Moreover, time-dependent susceptibility of Fe oxides to recrystallization dominates the reactivity of Fe(II)–Fe(III) atom exchange (Handler et al. 2014; Joshi et al. 2017; Notini et al. 2019b). During Fe(II)$_{aq}$-catalyzed recrystallization of goethite, the degree of Fe atom exchange between 1 and 30 days and between 30 and 60 days was investigated by conducting two batches of experiments (Joshi et al. 2017). The results showed that 17% of atoms in goethite undergo exchange with Fe(II)$_{aq}$ after 30 days of reaction, while only 2% of atoms in goethite undergo exchange with Fe(II)$_{aq}$ between 30 and 60 days. As a result, susceptibility of goethite to Fe(II)$_{aq}$-catalyzed

recrystallization appears to decrease over time. The observation from Joshi et al. (2017) is consistent with Notini et al. (2019b), which presented that a passivation layer accumulates from pre-exposed $Fe(II)_{aq}$ onto the Fe oxide surface and inhibits the extents of atom exchange over time. In addition, based on the theory model developed by Joshi et al. (2022), the resulting recrystallization of goethite in the presence of $Fe(II)_{aq}$ is markedly less than previously reported (14–20% vs 60–100%). This is because the majority of lattice Fe(III) in recrystallized goethite (> 80%) back-reacts slowly with $Fe(II)_{aq}$ (Joshi et al. 2022), whereas the previous studies assumed that the lattice Fe(III) in goethite back-reacts instantaneously (Handler et al. 2014; Latta et al. 2012a).

### 2.3 Isotopic exchange models

Although $Fe(II)_{aq}$-catalyzed recrystallization of Fe oxides has been extensively studied, a recrystallization model to ascribe the interfacial isotopic exchange at mineral–water interface remains unavailable. The homogenous and heterogeneous models were discussed in the literatures (Frierdich et al. 2019a; Handler et al. 2014). The primary difference between these two models, i.e., homogenous and heterogeneous models, is whether the bulk phases back-interact with $Fe(II)_{aq}$. The homogenous model deems that the recrystallized fraction of Fe oxide back-interacts with $Fe(II)_{aq}$, causing continuous and instantaneous Fe isotope fractionation at mineral–water interfaces during the entire reaction period (Handler et al. 2014). Therefore, in the homogenous model, the isotopic values of $Fe(II)_{aq}$ linearly approaches equilibrium. Alternatively, the heterogeneous model assumes that the recrystallized fraction of Fe oxide does not back-interact with $Fe(II)_{aq}$, and the recrystallized mineral from Fe(II) oxidation is accompanied by reductive dissolution of the initial mineral (Frierdich et al. 2014b, 2019a; Handler et al. 2014). Therefore, in the heterogeneous model, the isotope abundance of $Fe(II)_{aq}$ becomes close to that of the initial mineral over time. There are significant discrepancies in atom exchange ratios calculated by homogenous and heterogeneous models. For instance, the homogenous model suggests that 90% of Fe atom in goethite exchanges with Fe(II), while the heterogeneous model suggests only 19% in the same system (Handler et al. 2014; Joshi and Gorski 2016).

To evaluate whether the homogenous or heterogeneous models can fit the isotopic exchange approaches during recrystallization, Frierdich et al. (2019a) designed a three-isotope method ($^{54}Fe$–$^{56}Fe$–$^{57}Fe$) to assess isotopic fractionation during isotopic exchange between $Fe(II)_{aq}$ and hematite. Two $Fe(II)_{aq}$ solutions with different $\delta^{56/54}Fe$ ($Fe(II)_{aq}$ SS-1 and $Fe(II)_{aq}$ SS-2) were respectively reacted with hematite, and the isotopic fractionation in aqueous and solid phases was tracked by measuring $\delta^{57/56}Fe$ (Frierdich et al. 2019a). Based on results of three-isotope study (Frierdich et al. 2019a), at an early stage of the reaction, heterogeneous exchange of hematite with $Fe(II)_{aq}$ leads to the isotopic value of $\delta^{56/54}Fe$ of $Fe(II)_{aq}$ approaching initial hematite. Later on, $\delta^{56/54}Fe$ of $Fe(II)_{aq}$ exhibits an inflective trajectory with more negative values following continuous isotopic exchange. These data suggested that the rapid heterogeneous recrystallization changes to slow homogenous recrystallization over time, making the $\delta^{56/54}Fe$ of $Fe(II)_{aq}$ approaching the equilibrium fractionation value at the end of the reaction (Frierdich et al. 2019a).

## 3 Mineralogical recrystallization of Fe oxides

Mineralogical recrystallization of Fe oxides is also a primary process, in addition to the redox cycling and atom exchange between $Fe(II)_{aq}$ and Fe(III) in Fe oxides. Note that mineralogical recrystallization is defined as the crystal growth of Fe minerals with the same or different structure (Gorski and Fantle 2017; Yund and Tullis 1991). When exposed to $Fe(II)_{aq}$, amorphous ferrihydrite can quickly convert to a phase with higher crystallinity, such as goethite and magnetite (Liu et al. 2016; Williams and Scherer 2004). Different from poorly crystalline minerals, no new mineral phase is produced in suspensions involving crystalline Fe oxides such as goethite, hematite, and magnetite when exposed to $Fe(II)_{aq}$ (Frierdich et al. 2015a; Gorski et al. 2012; Handler et al. 2009). This phenomenon was previously described as simple Fe(II) adsorption–desorption (Zinder et al. 1986). Afterwards, new evidences from more advanced methods, including Fe isotope tracer, $^{57}Fe$-Mössbauer spectroscopy, and APT, reveal redox cycling between $Fe(II)_{aq}$ and crystalline Fe oxide phases

(Handler et al. 2009; Taylor et al. 2019a). Despite no phase transformation, some minor changes occur in the morphology and mineralogy of crystalline Fe oxides (e.g., crystallite size, surface defective extent, and Morin transition temperature) after reacted with $Fe(II)_{aq}$ (Joshi and Gorski 2016; Notini et al. 2018; Yanina and Rosso 2008). In addition, numerous studies identified the formation of intermediate phase, such as labile Fe(III) intermediates, lepidocrocite and goethite, which indicates the mass transfer pathways of Fe atoms during $Fe(II)_{aq}$-catalyzed recrystallization (Boland et al. 2014; Karimian et al. 2017; Sheng et al. 2020b). Here we discuss (1) the mineral variations during recrystallization and (2) the intermediate phases of recrystallization.

### 3.1 Mineral variations during recrystallization

Ferrihydrite is an amorphous Fe oxide that readily forms as the first mineral product of rapid Fe(III) hydrolysis, or $Fe(II)_{aq}$ oxidation, and polymerization (Cornell and Schwertmann 2004; Sheng et al. 2020b). Once exposed to $Fe(II)_{aq}$, ferrihydrite converts to lepidocrocite and/or goethite over a couple of days (Fig. 4) (Boland et al. 2013, 2014). Higher density of solid-associated Fe(II) enhances goethite growth, while less sorption of $Fe(II)_{aq}$ leads to slower lepidocrocite growth rates (Li et al. 2022; Sheng et al. 2020b; Shu et al. 2019). In contrast, ferrihydrite without $Fe(II)_{aq}$ has no observable phase transformation over the same period. Except for lepidocrocite or goethite, magnetite phase can also form from recrystallization of ferrihydrite when the $Fe(II)_{aq}$ density is relative high ($\geq$ 1 mmol Fe(II)/g ferrihydrite) (Hansel et al. 2005; Liu et al. 2016). Combination of $Fe(II)_{aq}$ adsorption and structural transformation of ferrihydrite is responsible for the heterogeneous growth of magnetite on ferrihydrite surface (Hansel et al. 2005). Moreover, lepidocrocite is also a thermodynamically metastable mineral in the environment (Cornell and Schwertmann 2004). Phase transformation of lepidocrocite to goethite in the presence of $Fe(II)_{aq}$ is also observed (Hansel et al. 2005; Wang and Giammar 2015).

As for the phase of secondary mineral after recrystallization, goethite is known as the more common secondary mineral relative to lepidocrocite and magnetite (Boland et al. 2013; Hansel et al. 2005). Hematite is rarely reported as the secondary mineral during recrystallization under room temperatures because higher pressures and/or temperatures are required for the nucleation of hematite (Cornell and Schwertmann 2004; Liu et al. 2007; Schwertmann 1983; Teja and Koh 2009). Liu et al. (2007) documented that high temperatures (> 60 ℃) facilitate the formation of hematite during $Fe(II)_{aq}$-catalyzed recrystallization of

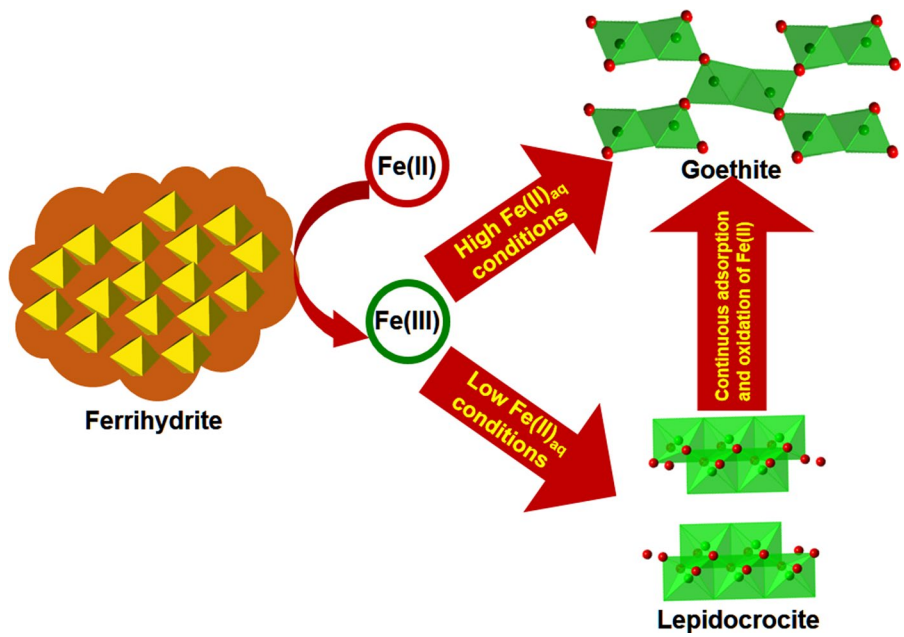


**Fig. 4** Overview of proposed mechanistic model of ferrihydrite recrystallization in the presence of $Fe(II)_{aq}$. Lepidocrocite growth is enhanced at lower $Fe(II)_{aq}$ concentrations while conditions leading to more rapid adsorption of $Fe(II)_{aq}$ from solution lead to quicker goethite growth from either ferrihydrite or lepidocrocite. The figure is reproduced from Boland et al. (2014), with permission from ACS publication

ferrihydrite. Beside these experimental observations, calculation of thermodynamic driving forces and nucleation energy barriers for magnetite precipitation from ferrihydrite transformation has been reported in literature (Li et al. 2022). The computational results provided a new insight into the phase stability and crystallization pathways of Fe oxides during $Fe(II)_{aq}$-catalyzed recrystallization (Li et al. 2022).

Furthermore, $Fe(II)_{aq}$-catalyzed recrystallization of crystalline Fe oxides can result in the changes of Fe oxide morphology and mineralogy, such as the crystallite size, defective extent, and Morin transition temperature (Joshi and Gorski 2016; Larese-Casanova and Scherer 2007b; Yanina and Rosso 2008). Joshi and Gorski (2016) reported that polycrystalline goethite particles consisting of smaller crystallites undergo a preferential increase in the mean particle width when exposed to $Fe(II)_{aq}$. Southall et al. (2018) also observed that the sizes of goethite crystallites (width of sub-units that comprise the larger particles) increased during the $Fe(II)_{aq}$-catalyzed recrystallization. Surfaces at goethite tips are prone to reductive dissolution, while the nucleation and growth of Fe(III) to neo-formed goethite preferentially occur along the crystallite boundaries (Zarzycki et al. 2015a).

In addition to the crystallite sizes, the defective extent and surficial morphology of Fe oxide may change during recrystallization. For instance, if an Fe oxide particle containing defects, $Fe(II)_{aq}$-catalyzed recrystallization of Fe oxide would preferentially smooth the surface defects (Notini et al. 2018, 2019b). Because Fe(II) oxidation on surface defects is more favorable than perfect surface (Notini et al. 2019b). When exposed to $Fe(II)_{aq}$, the recrystallization of coupled growth and dissolution on different hematite facets is observed (Rosso et al. 2010; Taylor et al. 2018; Yanina and Rosso 2008). The dissolution of edge surfaces is linked to simultaneous growth of the crystallographically distinct (001) basal plane (Rosso et al. 2010; Yanina and Rosso 2008).

Furthermore, based on Mössbauer spectra, Wu et al. (2021) suggested that hematite can undergo Morin transition suppression after reacted with $Fe(II)_{aq}$, which is consistent with previous research (Larese-Casanova and Scherer 2007a). This is because the injected electrons that donated from Fe(II) can be localized within the Fe(III) atom in hematite, which can result in the Morin transition suppression of hematite phase (Larese-Casanova and Scherer 2007b; Wu et al. 2021).

### 3.2 Intermediate phases of recrystallization

During recrystallization, the intermediate phases, such as labile Fe(III) intermediates, lepidocrocite and goethite, play a critical role in indicating the mass transfer pathways of Fe atoms. The labile Fe(III) intermediates originated from $Fe(II)_{aq}$ oxidation are believed to control the kinetics of mineralogical recrystallization of Fe oxide (Sheng et al. 2020a, b, 2021). Using a selective extractant (xylenol orange), Sheng et al. (2020a) isolated the labile Fe(III) intermediates from the Fe(II)-ferrihydrite suspensions and determined the recrystallization kinetics. Their results suggested that the temporal accumulation and consumption of labile Fe(III) are directly linked to the formation of secondary mineral outcomes (Sheng et al. 2020b). During $Fe(II)_{aq}$-catalyzed transformation of ferrihydrite, the labile Fe(III) intermediates assemble into goethite/lepidocrocite nuclei in a manner of olation and oxolation reactions (Sheng et al. 2020a). In addition, pre-existing Fe oxides can function as template for the heterogeneous aggregation growth of labile Fe(III) intermediate during $Fe(II)_{aq}$-catalyzed recrystallization (Notini et al. 2022). For instance, pre-existing goethite or magnetite facilitate the labile Fe(III) intermediate to assemble into new goethite or magnetite in the Fe(II)-lepidocrocite system (Notini et al. 2022; Sheng et al. 2021).

Besides, a myriad of research documented $Fe(II)_{aq}$-catalyzed recrystallization of ferrihydrite to magnetite, via lepidocrocite and/or goethite intermediates, which is coincident with Classical Nucleation Theory (Boland et al. 2014; Zhang et al. 2019). Lower Fe(II) surface loadings on ferrihydrite are more favorable for formation of lepidocrocite than goethite, and lepidocrocite can further convert to goethite then to magnetite when exposed to $Fe(II)_{aq}$ continuously (Boland et al. 2014).

## 4 Contributing factors of $Fe(II)_{aq}$-catalyzed recrystallization

The contributing factors on of Fe(II)–Fe(III) electron and atom exchange have been widely investigated. For instance, the initial Fe(II) concentration

is reported to dominate the rates and products of $Fe(II)_{aq}$-catalyzed recrystallization (Handler et al. 2009; Kang et al. 2018). Moreover, the rate of Fe atom exchange between Fe oxide and $Fe(II)_{aq}$ is restricted at lower pH and increased with the increase in pH (Hansel et al. 2005; Reddy et al. 2015). In addition to initial Fe(II) concentration and pH, the effects of light irradiation (Shu et al. 2019), anionic ligands (e.g., phosphate, sulfate, and silicate) (Borch et al. 2007; Jang et al. 2003; Jones et al. 2009), and organic contaminants (Cao et al. 2019; Klausen et al. 1995), on recrystallization kinetics are also investigated. Among these contributing factors, we focus on the mineralogical characteristics of Fe oxide such as mineral identity, grain size, crystallinity, and crystal facet as well as typical environmental factors including pH, initial Fe(II) concentration, metal(loid), OM, and microorganism as the representative factors since they have attracted the most extensive attentions in this field (Bao et al. 2021; Latta et al. 2012a; Reddy et al. 2015; Southall et al. 2018).

### 4.1 Mineralogical characteristics of Fe oxides

The identity of the initial Fe mineral greatly impacts the degree of electron and atom exchange during $Fe(II)_{aq}$-catalyzed Fe oxide recrystallization (Frierdich et al. 2015a, b; Reddy et al. 2015; ThomasArrigo et al. 2017). Ferrihydrite can undergo almost 100% atom exchanges with Fe(II) and subsequently complete phase transformation to goethite and lepidocrocite over a couple of days (ThomasArrigo et al. 2017). As for goethite, 68% of Fe atoms undergoes atom exchanges with $Fe(II)_{aq}$ at pH 7.5 after 50 days (Reddy et al. 2015). Under comparable conditions, Frierdich et al. (2015b) disclosed 25% of Fe in hematite can undergo exchanges with aqueous Fe(II) over 30 days, and Gorski et al. (2012) found that only 10% of Fe atom in magnetite undergoes exchange with $Fe(II)_{aq}$, which is close to the monolayer coverage of magnetite surface. These results showed that when exposed to $Fe(II)_{aq}$, poorly crystalline Fe oxides would undergo more extensive and faster recrystallization compared with crystalline Fe oxides. This is mainly because that Fe oxides with smaller crystallites have more surface area and sites to connecting with $Fe(II)_{aq}$ (Gorski et al. 2012; Reddy et al. 2015).

In addition, $Fe(II)_{aq}$-catalyzed recrystallization is regulated by mineral surface natures (e.g., grain size, specific surface area, and crystallinity) of the Fe oxides. For instance, Frierdich et al. (2015b) reported that 50 nm-hematite (54 $m^2\ g^{-1}$) experiences ~ 25% of atom exchanges with Fe(II), while 80 nm-hematite (27 $m^2\ g^{-1}$) only experiences ~ 5% under the same conditions. By comparing the recrystallized extents of goethite with different crystallites, Southall et al. (2018) found that the goethite with 10 nm crystallite sizes undergoes more atom exchanges with Fe(II) (~ 80% of exchange) relative to the goethite with 26 nm crystallite sizes (~ 10% of exchange). Similar changes in morphology of individual goethite particle are also observed in both scanning electron microscope (SEM) and transmission electron microscope (TEM) images (Joshi and Gorski 2016). Fe oxides with smaller particle and crystallite sizes usually exhibit a higher specific surface area, leaving more surface sites to interact with $Fe(II)_{aq}$ (Frierdich et al. 2015b; Southall et al. 2018).

Regarding the facet-selectivity of the crystal grain, the types and proportion of facets exposed to the solution control the reactivity of the mineral (Gaboriaud and Ehrhardt 2003; Hu et al. 2021; Huang et al. 2018; Lv et al. 2018; Weidler et al. 1998). As shown in Fig. 5A–C, different facets of a singular hematite crystal exhibit different reactivity to Fe(II), and surface dissolution of hematite (*h k* 0) edge play a critical role in the coinstantaneous growth of the structurally different (0 0 1) plane facet (Yanina and Rosso 2008). Using nanoscale secondary ion mass spectrometry (nano-SIMS), Taylor et al. (2019b) visualized and quantified Fe isotopic distribution at the interface of a $^{57}Fe(II)_{aq}$ and $^{56}$Fe-hematite system. The $^{57}Fe/^{56}Fe$ ratios of hematite become higher after reacting with $^{57}Fe(II)_{aq}$, with the $^{57}Fe/^{56}Fe$ ratio of the basal {001} facet significantly exceeding the ratios of the {110} and {012} edge facets (up to 10 times higher) (Fig. 5D, E). These results demonstrated a strong selectivity of Fe(II) adsorption onto the hematite basal {001} surface, which is consistent with the previous observations when various single crystal surfaces were used to absorb $Fe(II)_{aq}$ (McBriarty et al. 2018; Yanina and Rosso 2008).

The reason of facet-selectivity of crystal on $Fe(II)_{aq}$-catalyzed recrystallization is that the different crystal facets exhibit different Gibbs free energies to Fe(II) adsorption (Taylor et al. 2019a). The connection of $Fe(II)_{aq}$ with hematite {001} facet appears to be a more stable structure with lower energy relative

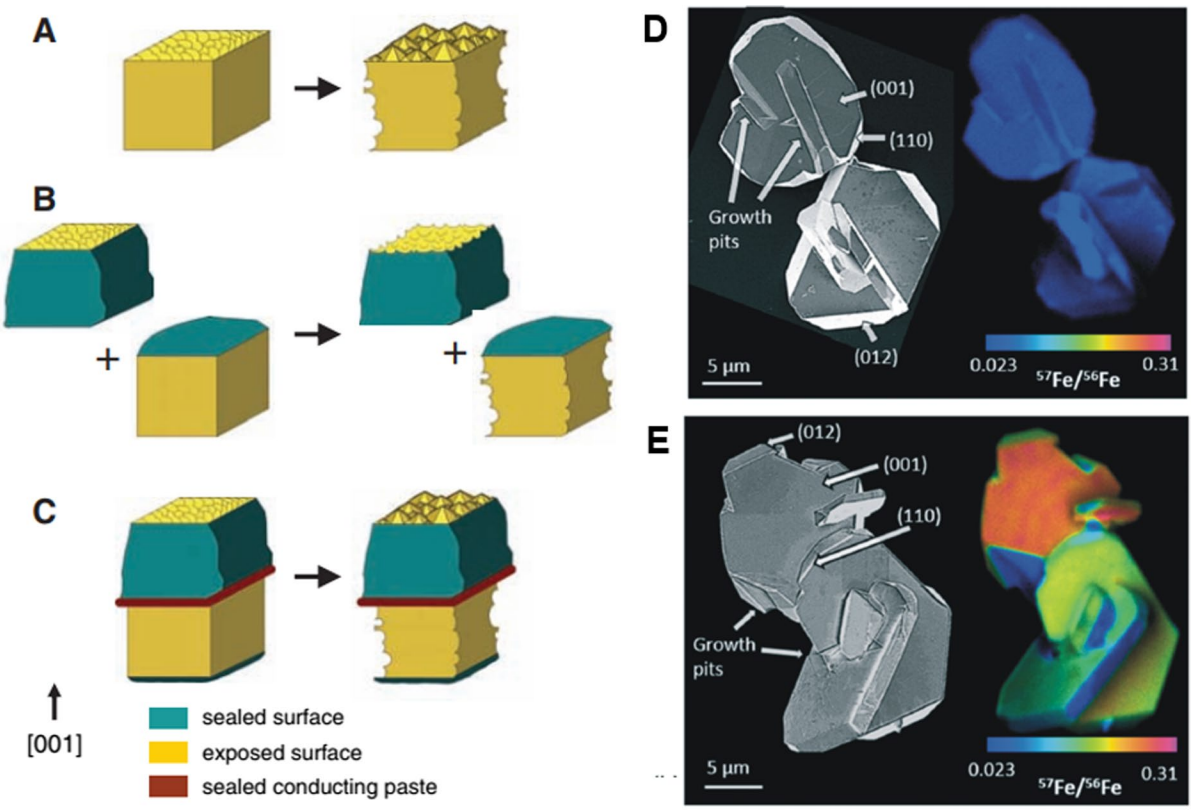


**Fig. 5** Schematic diagram summarizing the observed reaction behavior of hematite crystals and showing **a** (001) pyramidal growth coupled to (*hk*0) dissolution; **b** (001) and (*hk*0) dissolution for selectively sealed two-crystal cases where the same surface area and type as in (**a**) are exposed to solution; and **c** (001) pyramidal growth coupled to (*hk*0) dissolution facilitated by a conducting paste connection between two crystals (Yanina and Rosso 2008). Copyright 2008, with permission from American Association for the Advancement of Science. SEM and 57Fe/56Fe maps from nanoscale secondary ion mass spectrometry (nano-SIMS) on **d** unreacted and **e** reacted hematite particles. This figure is adopted from Taylor et al. (2019a, b). Copyright 2019, with permission from Royal Society of Chemistry

to {012} and {110} facets. Therefore, $Fe(II)_{aq}$-catalyzed recrystallization of Fe oxide proceeds more extensively on the reactive facet of the mineral crystal. However, in Wu et al. (2021) hematite {012} was identified to exhibit stronger reactivity to Fe(II) than hematite {001} during $Fe(II)_{aq}$-catalyzed recrystallization of two hematite facets. The facet-specific reactivity is attributed to the density and coordination conditions of surface Fe atoms (Wu et al. 2021). The contradictory conclusions obtained from Taylor et al. (2019a) and Wu et al. (2021) might be a result of the use of different morphological hematite grains, although further evidence is needed.

The exchange rate and degree between $Fe(II)_{aq}$ and Fe mineral are linked to the density of surficial defects (Russell et al. 2009; Southall et al. 2018). $Fe(II)_{aq}$-catalyzed recrystallization in accompany with elimination of the defective surficial sites form a more perfect surface is believed to act as the energetic driving force for Fe(II)–Fe(III) atom exchange (Notini et al. 2018). Defective surficial sites enhanced $Fe(II)_{aq}$ adsorption and electron injection into the surficial Fe lattice, which results in the minimization of surficial potential energy of Fe oxide (Alexandrov and Rosso 2015; Notini et al. 2018). Using $^{57}$Fe Mössbauer spectra, Notini et al. (2018) found that ground goethite with a defective grain surface can oxidize more $^{57}$Fe(II) to $^{57}$Fe-goethite relative to goethite with a perfect surface. Based on APT, $Fe(II)_{aq}$-catalyzed recrystallization is documented to be a highly spatially heterogeneous process (Taylor et al. 2019b). The defective sites of Fe exhibit higher

reactivity compared with perfect sites on the goethite surface. Using novel molecular simulation methods, Zarzycki and Rosso (2019) suggested that defective surface accelerates atom exchange relative to the perfect surface via accessing the intra surface electron conduction pathways of 2 nm up to 8 nm (Zarzycki and Rosso 2019).

### 4.2 Typical environmental factors

It has been widely observed that increasing pH or initial $Fe(II)_{aq}$ concentrations can notably promote Fe(II)-catalyzed recrystallization (Frierdich et al. 2015b; Li et al. 2022; Liu et al. 2016; Sheng et al. 2020b). There are three possible reasons to explain why pH and initial $Fe(II)_{aq}$ concentrations significantly affect Fe atom exchange and mineral transformation.

Firstly, pH controls the extent of Fe(II) adsorption onto Fe oxides (Frierdich et al. 2015b). As a typical cation adsorption process, the amount of adsorbed Fe(II) on Fe oxides increases with the increase in pH (Frierdich and Catalano 2012; Reddy et al. 2015). The accumulation of surficial Fe(II) on Fe oxide minerals accelerates Fe atom exchange and phase transformation (Handler et al. 2014).

Secondly, pH alters the driving force for interfacial Fe(II)–Fe(III) electron transfer (Reddy et al. 2015; Zarzycki and Rosso 2018). The geometry of the Fe(II)–Fe(III) surficial complex depends on pH: when pH of the system is above the point of zero charge (PZC) of the Fe oxide, an Fe(II)–Fe(III) inner-sphere complex is formed on the negatively charged surface; when pH is below the PZC, an outer-sphere complex is formed on the positively charged surface (Zarzycki and Rosso 2018). Because the pH dependence of surficial complex geometry impacts the distance and energetics for Fe(II)–Fe(III) electron transfer, pH can strongly regulate the rate and extent of $Fe(II)_{aq}$-induced recrystallization of Fe oxides.

Lastly, pH impacts the identity of secondary mineral products from $Fe(II)_{aq}$-catalyzed transformation of ferrihydrite (Jang et al. 2003; Li et al. 2022). Based on Classical Nucleation Theory, Li et al. (2022) developed a unifying model that discloses the effects of pH and redox conditions on thermodynamic driving forces and nucleation energy barriers of ferrihydrite transformation. Their modeling results demonstrated that the thermodynamic driving forces and nucleation energy barriers for the transformation from ferrihydrite to magnetite decrease with increase of pH, but those for lepidocrocite, goethite or hematite are constant over pH range 6.0–8.0 (Li et al. 2022). Moreover, the energy barriers for magnetite transformation are lower than that for goethite transformation at $pH > 7.0$, leading to more magnetite precipitation from $Fe(II)_{aq}$-catalyzed ferrihydrite transformation in alkaline systems (Li et al. 2022).

Nevertheless, excessive Fe(II) on surface of Fe oxide may modify the electrostatic surface potential (Yanina and Rosso 2008), and then inhibits Fe atom exchange between $Fe(II)_{aq}$ and Fe(III) in Fe oxide. Once the amount of added Fe(II) exceeds the monolayer coverage of Fe oxide, interfacial Fe(II)–Fe(III) electron transfer is inhibited because the excessive Fe(II) changes the bulk conduction and neutralized the surface potential gradient of the mineral (Frierdich et al. 2015b; Yanina and Rosso 2008). For example, even when the amount of sorbed Fe(II) onto hematite reaches ~ 4 mM, only ~ 9% of Fe(III) in hematite, i.e., approximately a singular layer, undergoes atom exchange with the Fe(II) (Frierdich et al. 2015b). In addition, less Fe atom undergoes exchange between $Fe(II)_{aq}$ and hematite at pH 8.0 compared to pH 7.5, even though the measured amount of Fe(II) adsorption at pH 8.0 exceeds the surface site capacity of Fe oxides in theory (Frierdich et al. 2015b).

In natural environments, many metal(loid)s coexist with $Fe(II)_{aq}$ and Fe oxide and affect $Fe(II)_{aq}$-catalyzed Fe oxide recrystallization (Fig. 6). Previous studies shown that the presence of magnesium (Mg), calcium (Ca), zinc (Zn), barium (Ba), nickel (Ni), aluminum (Al), uranium (U), and arsenic (As) can slow down the $Fe(II)_{aq}$-catalyzed Fe oxide recrystallization (Boland et al. 2011; Jang et al. 2003; Latta et al. 2012a; Liu et al. 2016; Massey et al. 2014; Perez et al. 2019). The competitive adsorption of metal(loid)s decrease reactive surface sites favorable for Fe(II) and thereby inhibite the electron and atom exchange and mineral recrystallization (Das et al. 2011). Additionally, the presence of As(V) is reported to inhibit $Fe(II)_{aq}$-catalyzed recrystallization though formation of symplesite, a ferrous arsenate mineral (Catalano et al. 2011). Also, Latta et al. (2012a) indicated that pure goethite undergoes ~ 40% of atom exchange with Fe(II), whereas Al-substituted goethite only undergoes ~ 10% under the same condition. Both incorporated and solid-associated metal(loid)s can

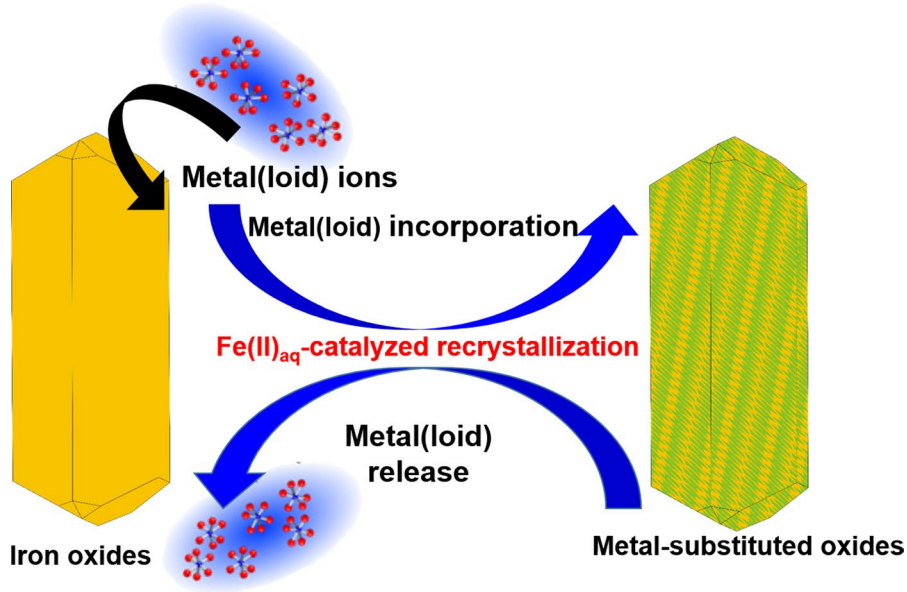


**Fig. 6** Schematic representation of incorporation and release cycling of metal(loid)s across mineral–water interfaces during the $Fe(II)_{aq}$-catalyzed Fe oxide recrystallization

hinder the conversion of ferrihydrite to other Fe minerals through the formation of a metal(loid)-coating, thus blocking the reactive sites and preventing the dissolution of Fe oxides (Ekstrom et al. 2010).

In addition to metal(loid)s, Fe oxides also have a high affinity for OMs (Chen and Thompson 2021; Redman et al. 2002). Chen et al. (2015) reported that the rate and degree of mineral phase conversion of OM-ferrihydrite decreased with increasing C/Fe ratios, suggesting that phase transformation is limited by OM coprecipitation (Chen et al. 2015; Jones et al. 2009; Noor and Thompson 2022). Three interpretations are proposed in the literature to explain why OM coprecipitation inhibits the degree of $Fe(II)_{aq}$-catalyzed recrystallization (Fig. 7). Firstly, the competitive adsorption between Fe(II) and OMs results in less Fe(II) adsorption on Fe oxides (Jones et al. 2009). Secondly, $Fe(II)_{aq}$ can be stabilized by the formation of Fe(II)-OM solution complexes and further restricts the adsorption of Fe(II) (ThomasArrigo et al. 2017). Thirdly, the incorporation of OMs into pores and/or lattices of the Fe oxides

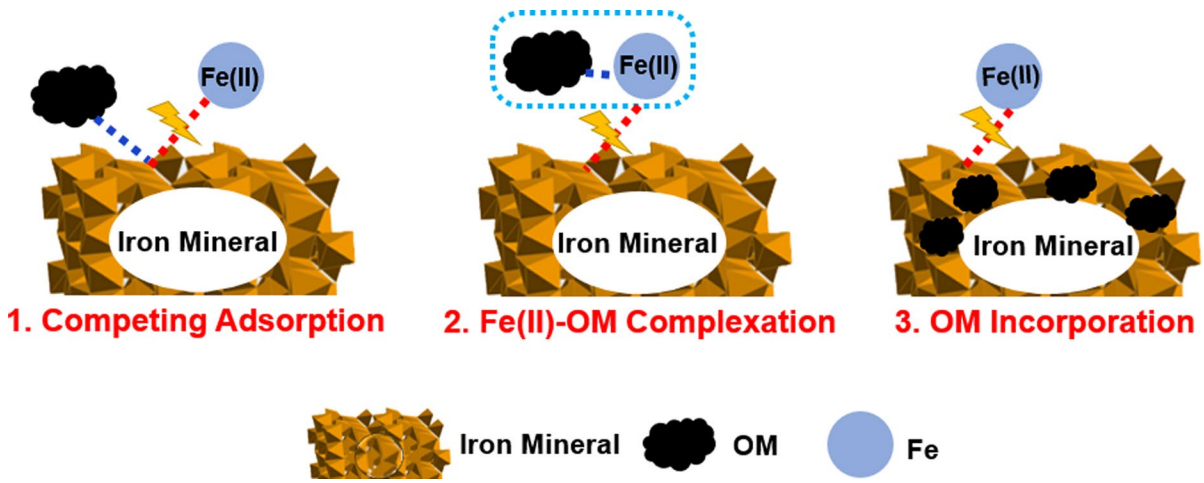


**Fig. 7** Three probable interpretations for the inhibition of OMs on the $Fe(II)_{aq}$-catalyzed Fe oxide recrystallization

hinders the recrystallization process of Fe oxides (Xiao et al. 2018).

Numerous studies indicated that OMs can inhibit the phase transformation during $Fe(II)_{aq}$-catalyzed ferrihydrite recrystallization. Despite no apparent phase transformation, Zhou et al. (2018) found that interfacial electron transfer still occurs between the adsorbed Fe(II) and OM-ferrihydrite coprecipitations based on Fe isotope tracer and $^{57}Fe$ Mössbauer spectra. The macromolecular OMs are believed to obstruct the nanocluster movement and arrangement, thereby inhibiting the aggregation and generation of bigger crystals (ThomasArrigo et al. 2018). In this case, ferrihydrite in OM-ferrihydrite coprecipitation can only transform to less crystalline Fe minerals, such as "new" ferrihydrite and nanoclusters of lepidocrocite-like structure, rather than goethite and magnetite, which are the common mineral products in pure ferrihydrite experiments (Zhou et al. 2018). The negative surficial charge from OM coprecipitation also prevents oriented aggregation growth of ferrihydrite, because the crystal growth and aggregation are enhanced only when the surface charge is close to the PZC of the mineral phase ($PZC_{ferrihydrite} \approx 7.0$) (Jones et al. 2009).

Microorganisms can function as a pump for Fe redox cycling and accelerate mineralogical recrystallization of Fe oxides (Fredrickson et al. 1998; Weber et al. 2006a). The influences from the cell density and ratio between electron donor and acceptor on the secondary mineral formation in the presence of the Fe(III)-reducing bacteria were also investigated (Fredrickson et al. 2003; Hansel et al. 2003; Lies et al. 2005; Piepenbrock et al. 2011; Xiao et al. 2018; Zachara et al. 2002). Hensel et al. (2003) evaluated the effect of microbial respiration on the rate of ferrihydrite transformation, and found that microbial Fe(III) reduction generates an increased amounts of Fe(II) and thereby boosts the transformation rate. In the presence of Fe(III)-reducing bacteria, ferrihydrite converts to less goethite and more lepidocrocite than that in the absence of microorganisms (Xiao et al. 2018). In addition, lower electron donor to acceptor ratios cause recrystallization of poorly crystalline Fe oxide to lepidocrocite and goethite, whereas higher ratios lead to rapid dissolution and/or the generation of siderite (Fredrickson et al. 2003).

In addition, biotic processes often have "vital effects", producing a larger discrepancy in isotope abundance relative to equilibrium isotope exchange in abiotic process (Beard et al. 2003). However, Crosby et al. (2005) found that the interfacial Fe(II)–Fe(III) atom exchange resulted in equivalent Fe isotope fractionations during both biotic and abiotic processes, suggesting that the isotope fractionation mechanisms are similar. Therefore, the presence of microbe in $Fe(II)_{aq}$-catalyzed recrystallization only leads to elevated production of Fe(II) without isotope fractionation (Crosby et al. 2005).

## 5 Analytical methodologies

Two broad categories of analytical methodologies are frequently employed in the field of $Fe(II)_{aq}$-catalyzed Fe oxide recrystallization (Table 1). First category of techniques, including isotope tracers, $^{57}Fe$ Mössbauer spectroscopy, and APT, are often employed to testify the redox cycling and isotope exchange between $Fe(II)_{aq}$ and Fe(III) in Fe oxides. Fe isotope tracers is a key technique that can determine the kinetics of Fe atom exchange, which can be used for comparing the effects of different influencing factors on recrystallization (Frierdich et al. 2015b; Handler et al. 2014). Isotope tracers can be used in combination with $^{57}Fe$ Mössbauer spectroscopy or APT to investigate recrystallization of Fe oxides. For example, Larese-Casanova et al. (2007a) identified that Fe atom undergoes rapid exchanges when $^{57}Fe(II)_{aq}$ reacted with $^{56}Fe$-hematite over a range of Fe(II) concentrations and pH values using Mössbauer spectra. $^{57}Fe$ Mössbauer spectroscopy is utilized to disclose the uniform $^{57}Fe$ speciation in Fe oxide, while APT can unravel a non-uniform Fe isotopic distribution in three dimensions (Frierdich et al. 2019b; Kim et al. 2019). As a mass-sensitive imaging technique, APT has high sensitivity and spatial resolution for directly mapping the atomic and isotopic distributions in mineral grains (Gault et al. 2009; Kim et al. 2019). Besides, APT is adapted to monitor $^{56}Fe/^{57}Fe$ distributions on individual Fe oxide crystallite at the atomic scale (Kim et al. 2019; Taylor et al. 2018, 2019b). $^{57}Fe$ Mössbauer, on the other hand, can also be used to distinguish Fe species because they would produce diverse peaks and fitting parameters, i.e., isomer shift ($\delta$) and quadrupole splitting ($\Delta$) (Larese-Casanova and Scherer 2007a).

**Table 1** Comparison of the technical background, functions, strengths and limitations of different analytical methodologies

| Methodology | Technical background | Functions | Strengths | Limitations | References |
|---|---|---|---|---|---|
| Isotope tracer | To trace the path and whereabouts of isotopes in a chemical reaction, metabolic pathway, or cellular localization | Quantifies the kinetics of Fe atom exchange, traced the isotopic equilibrium process and testified the isotopic exchange models | Is the only method that can quantify the atom exchange | Only provides a uniform Fe isotope data on account of its sample preparation | Frierdich et al. (2015b); Handler et al. (2014) |
| Atom probe tomography (APT) | To reconstruct the isotope/atom distribution of the bulk sample | Maps the atomic and isotopic distributions on cross-sections of the sample microrods for disclosing the non-uniform Fe isotope exchange | Has high sensitivity and spatial resolution and provides a non-uniform Fe isotope data in mineral bulk | Sample preparation is a great challenge | Kim et al. (2019); Taylor et al. (2018, 2019b) |
| $^{57}$Fe Mössbauer spectroscopy | To distinguish Fe species relied on γ-ray resonance absorption phenomenon without losing energy on recoil | Identifies the mineral phases for tracing the phase transformation during recrystallization | Has high resolution for identification of Fe oxides | Requires substantial effort to operate safely and also is high costs and the relatively narrow range of applications | Williams and Scherer (2004); Larese-Casanova and Scherer (2007a) |
| X-ray diffration (XRD) | To identify the composition of crystal phase by analyzing the emitted diffraction patterns from space lattice | Testifies the identification of mineral phases | Can be carried out with relatively low cost instrumentation requiring minimal safety precautions and, given its wide range of applications, is available in most research laboratories | Is not suitable for analyzing the poorly crystalline minerals or the recrystallization of iron oxide with the same structure | Hu et al. (2020); ThomasArrigo et al. (2018) |
| Scanning electron microscopy (SEM)/Transmission electron microscope (TEM) | To characterize surface topography of a solid material through scanning/transmitting the surface with a focused beam of electrons | Maps the subtle changes in mineral mineralogy and morphology for verifying the recrystallization even without phase transformation | Provides directly observations of mineral mineralogy and morphology | Is unfavorable for characterization of iron oxide recrystallization with same structure, and is not suitable for quantification of secondary formed minerals | Hansel et al. (2005); Joshi and Gorski (2016); Zong et al. (2019) |
| Fourier-transform infrared (FTIR) | Provided information of the principal chemical groups and mineral components of sample | Quantifies the mineral compositions | Provides rapid testing and bulk analyses of large sample number | Accurate identification of FTIR absorbance bands is hindered by mineral interference | Xiao et al. (2017); Xiao et al. (2018); Zhang et al. (2019) |

**Table 1** (continued)

| Methodology | Technical background | Functions | Strengths | Limitations | References |
|---|---|---|---|---|---|
| X-ray absorption fine structure (NEXAFS) | To characterize the speciation in complex systems on account of absorption spectra depend directly on the local bonding environment of atoms | Quantifies the mineral phases even in complex soil/sediment samples containing short-range-ordered minerals such as ferrihydrite | Is markedly sensitive to the bonding environment of the element of interest | This technique with less than 100 instruments worldwide is not readily available to most researchers and also requires immense safety precautions | Boland et al. (2013); Hu et al. (2020); Shu et al. (2019) |

Second category of techniques, such as X-ray diffraction (XRD), TEM, SEM, Fourier-transform infrared (FTIR) spectroscopy, and XAS are able to trace the mineralogical recrystallization of Fe oxides when exposed to $Fe(II)_{aq}$. XRD is able to identify the mineral compositions based on the diffraction patterns of space lattice in crystals. Numerous studies have documented the mineralogical conversion of Fe oxides in the presence of $Fe(II)_{aq}$ using XRD (Hu et al. 2020; Liu et al. 2019). The morphological natures of Fe oxides can also be used to identify the phase composition (Hansel et al. 2005; Joshi and Gorski 2016; Zong et al. 2019). Both TEM and SEM can be employed to monitor the mineralogical transformation of Fe oxide in this realm (Eusterhues et al. 2008; Joshi and Gorski 2016; Taylor et al. 2019a). SEM can provide information on topology while TEM provides insight into aspects such as crystallinity (Zong et al. 2019). XRD full-pattern fitting, FTIR, Fe extended X-ray absorption fine structure (EXAFS) and $^{57}Fe$ Mössbauer spectroscopy can be used to quantify the relative proportions of diffident Fe phases in Fe oxide after exposed to $Fe(II)_{aq}$. XRD full-pattern fitting with Rietveld refinements can be employed to calculate the relative mass of each phase identified in the mineral samples via analyzing integrated intensity of the diffraction peaks and the crystal structure (Aeppli et al. 2019; Liu et al. 2016; ThomasArrigo et al. 2018). But XRD full-pattern fitting is unfavorable for the recrystallization of Fe oxide with the same structure. FTIR can determine the relative ratio of Fe oxide in a mixed Fe oxide suspension based on the peak height of signature peaks of references minerals (Xiao et al. 2017, 2018; Zhang et al. 2019). However, the accurate identification of FTIR absorbance bands is often hindered by mineral interference (Wang et al. 2021). Moreover, EXAFS also allows the identification of various Fe phases and quantification of their relative proportions, typically by linear combinations of reference spectrum (Boland et al. 2013; Hu et al. 2020; Shu et al. 2019; Sun et al. 2018). Sun et al. (2018) confirmed the accuracy of EXAFS linear combination fitting for quantifying Fe mineral composition even in complex soil/sediment samples containing short-range-ordered minerals such as ferrihydrite.

## 6 Outlook

Current research in the field of $Fe(II)_{aq}$-catalyzed Fe oxide recrystallization have greatly improved our understanding of the Fe redox cycle and advanced our ability to predict the environmental behaviors of many other vital elements. Nevertheless, to roundly comprehend the details in $Fe(II)_{aq}$-catalyzed recrystallization of Fe oxides, continued research efforts are still warranted in several aspects. Disclosing the underlying mechanism of electron and atom exchange at Fe(II)–Fe(III) interfaces can help us to better understand Fe redox cycle in the environments. Previous theoretical studies disclosed the conversion of adsorbed Fe(II) from outer-sphere Fe(II) species to inner-sphere Fe(II) species before initiating the interfacial electron transfer, which is the first step in $Fe(II)_{aq}$-catalyzed recrystallization (Alexandrov and Rosso 2015; Zarzycki et al. 2015a, b). However, whether the formation of inner-sphere Fe(II) species is required to enable the interfacial electron transfer remains unclear.

Exploring the isotope characteristics of Fe oxide during recrystallization can help us understand the mechanism of mineral-fluid exchange (Frierdich et al. 2014a, b, 2019a). For example, it was reported that the location of isotope exchange inflection, i.e., change from heterogeneous to homogeneous exchange, is considered relevant to surficial sites on hematite during recrystallization, which can alter the isotopic composition of hematite accordingly (Frierdich et al. 2019b). Nevertheless, the role of other morphological natures, such as the crystal facet and crystallinity, in impacting the location of isotope exchange inflection is still unknown. Several previous research documented that the different exposed facets of Fe oxide exhibit unique reactivity to $Fe(II)_{aq}$-catalyzed recrystallization (Taylor et al. 2019b; Wu et al. 2021). Nonetheless, an in-depth investigation on the correlation between the exposed facets and isotope exchange models is still missing.

Intermediate Fe(IV) species is observed as an effective oxidant for toxic elements such as As(III) in previous research (Hug and Leupin 2003; Pestovsky and Bakac 2004; Qiu et al. 2017), which is detected by $^{57}$Fe-Mössbauer spectroscopy in Fe(II)-goethite suspension using a rapid freeze–quench technique (Hua et al. 2022). More evidences on the generation of Fe(IV) species during recrystallization are required for understanding and explaining anoxic oxidative transformation processes in non-surface environments. However, there is still a lack of application of the in situ spectroscopic technologies, such as in situ XAS and Mössbauer spectroscopy, to monitor the generation of intermediate Fe species. Since these intermediates are easily decomposed during sample preparation and handling (Hua et al. 2022; Pestovsky and Bakac 2004; Sheng et al. 2020b). The application of in situ spectroscopic technologies can provide new insights into the mechanism of production of the intermediate species during Fe oxide recrystallization in this realm.

Additionally, the isotopic compositions of Fe oxide are considered as a potential proxy for paleo-redox conditions and used to study the biogeochemical cycling of Fe in Earth history (Abrajevitch et al. 2009; Guo et al. 2013). Fe isotope fractionation is expected to be used to trace biological process of Fe cycling, as it may produce a unique isotopic value different from that in abiotic process (Beard et al. 2003). However, Crosby et al. (2005) found that the $Fe(II)_{aq}$ produced from dissimilatory microbial Fe(III) reduction exhibits the same isotopic ratio with the $Fe(II)_{aq}$ that undergoes abiotic exchange with Fe oxide. Thereby, microbial Fe reduction may not change the isotopic ratio of Fe(II) reduced from Fe oxides. Nevertheless, direct measurement on isotopic ratio of the un-exchanged Fe(II) remains missing, because the formed Fe(II) undergoes quick and sustaining exchange with the Fe(III) in Fe oxide.

Lastly, although considerable progress has been made in understanding the effects of various environmental factors on $Fe(II)_{aq}$-catalyzed Fe oxide recrystallization, the complexity of natural systems still results in a lack of anticipation tools by far. The majority of current experimental investigations are limited to single, well-defined Fe oxide, and often only involve either metal(loid)s or OMs. However, in natural environments, Fe oxides coexist with other Fe mineral phases and a mixture of other environmental variables including organic and inorganic pollutants, nutrients and trace elements (Bao et al. 2021; Eglinton 2012; Huang et al. 2021; Tishchenko et al. 2015). A unifying modeling framework developed by Li et al. (2022) that can be used to predict the kinetics and pathways of Fe oxide transformation under a series of pH and redox conditions. However, a theoretical model concerning more environmental

substances such as metal(loid)s and organic carbon effects on the stabilities and transformation of Fe oxides remains missing. Overall, more experimental and theoretical studies are needed to explain how a variety of Fe minerals coexisting with different microbial and/or chemical species affect the process of $Fe(II)_{aq}$-catalyzed Fe oxide recrystallization.

**Acknowledgements** This study was supported by the National Natural Science Foundations of China (41921004 and 42025705); the West Light Foundation and the Frontier Science Research Programme of the Chinese Academy of Sciences (QYZDB-SSW-DQC046); the Science and Technology Planning Project of Guangdong Province, China (2019GDSYL-0401003 and 2019GDASYL-0301002).

**Author contributions** JH: conceptualization, manuscript writing—original draft, writing—review and editing. JS: supervision, writing—review and editing, validation. MJC: supervision, validation. CSL: project administration, funding acquisition, writing—review and editing, validation. FW: writing—review and editing, validation. All authors read and approved the final manuscript.

**Declarations**

**Conflict of interest** The authors declare that they have no potential conflict of interest with respect to the research, authorship or publication of this article.

## References

Abrajevitch A, Van der Voo R, Rea DK (2009) Variations in relative abundances of goethite and hematite in Bengal Fan sediments: climatic vs. diagenetic signals. Mar Geol 267(3–4):191–206. https://doi.org/10.1016/j.margeo.2009.10.010

Aeppli M, Vranic S, Kaegi R, Kretzschmar R, Brown AR, Voegelin A, Hofstetter TB, Sander M (2019) Decreases in iron oxide reducibility during microbial reductive dissolution and transformation of ferrihydrite. Environ Sci Technol 53(15):8736–8746. https://doi.org/10.1021/acs.est.9b01299

Alexandrov V, Rosso KM (2014) Electron transport in pure and substituted iron oxyhydroxides by small-polaron migration. J Chem Phys 140(23):234701. https://doi.org/10.1063/1.4882065

Alexandrov V, Rosso KM (2015) Ab initio modeling of Fe(II) adsorption and interfacial electron transfer at goethite (a-FeOOH) surfaces. Phys Chem Chem Phys 17(22):14518–14531. https://doi.org/10.1039/c5cp00921a

Balogh E, Todea AM, Muller A, Casey WH (2007) Rates of ligand exchange between > Fe-III-OH2 functional groups on a nanometer-sized aqueous cluster and bulk solution. Inorg Chem 46(17):7087–7092. https://doi.org/10.1021/ic7009308

Bao YP, Bolan NS, Lai JH, Wang YS, Jin XH, Kirkham MB, Wu XL, Fang Z, Zhang Y, Wang HL (2021) Interactions between organic matter and Fe (hydr)oxides and their influences on immobilization and remobilization of metal(loid)s: a review. Crit Rev Environ Sci Technol. https://doi.org/10.1080/10643389.2021.1974766

Beard BL, Johnson CM, Skulan JL, Nealson KH, Cox L, Sun H (2003) Application of Fe isotopes to tracing the geochemical and biological cycling of Fe. Chem Geol 195(1–4):87–117. https://doi.org/10.1016/s0009-2541(02)00390-x

Boland DD, Collins RN, Payne TE, Waite TD (2011) Effect of amorphous Fe(III) oxide transformation on the Fe(II)-mediated reduction of U(VI). Environ Sci Technol 45(4):1327–1333. https://doi.org/10.1021/es101848a

Boland DD, Collins RN, Glover CJ, Waite TD (2013) An in situ quick-EXAFS and redox potential study of the Fe(II)-catalysed transformation of ferrihydrite. Colloid Surf A 435(130):2–8. https://doi.org/10.1016/j.colsurfa.2013.02.009

Boland DD, Collins RN, Miller CJ, Glover CJ, Waite TD (2014) Effect of solution and solid-phase conditions on the Fe(II)-accelerated transformation of ferrihydrite to lepidocrocite and goethite. Environl Sci Technol 48(10):5477–5485. https://doi.org/10.1021/es4043275

Borch T, Masue Y, Kukkadapu RK, Fendorf S (2007) Phosphate imposed limitations on biological reduction and alteration of ferrihydrite. Environ Sci Technol 41(1):166–172. https://doi.org/10.1021/es060695p

Brown GE, Henrich VE, Casey WH, Clark DL, Zachara JM (1999) Metal oxide surfaces and their interactions with aqueous solutions and microbial organisms. Chem Rev 30(1):77. https://doi.org/10.1021/cr980011z

Cao J, Huang J, Dong H, Li J, Shou J, Li Y (2019) Effects of surfactants on the removal of nitrobenzene by Fe(II) sorbed on goethite. J Colloid Interface Sci 552:764–770. https://doi.org/10.1016/j.jcis.2019.05.095

Catalano JG, Fenter P, Park C, Zhang Z, Rosso KM (2010) Structure and oxidation state of hematite surfaces reacted with aqueous Fe(II) at acidic and neutral pH. Geochim Cosmochim Acta 74(5):1498–1512. https://doi.org/10.1016/j.gca.2009.12.018

Catalano JG, Luo Y, Otemuyiwa B (2011) Effect of aqueous Fe(II) on arsenate sorption on goethite and hematite. Environ Sci Technol 45(20):8826–8833. https://doi.org/10.1021/es202445w

Chen CM, Thompson A (2021) The influence of native soil organic matter and minerals on ferrous iron oxidation. Geochim Cosmochim Acta 292:254–270. https://doi.org/10.1016/j.gca.2020.10.002

Chen CM, Dynes JJ, Wang J, Sparks DL (2014) Properties of Fe-Organic matter associations via coprecipitation versus adsorption. Environ Sci Technol 48(23):13751–13759. https://doi.org/10.1021/es503669u

Chen CM, Kukkadapu RK, Sparks DL (2015) Influence of coprecipitated organic matter on Fe2+(aq)-catalyzed transformation of ferrihydrite: implications for carbon dynamics. Environ Sci Technol 49(18):10927–10936. https://doi.org/10.1021/acs.est.5b02448

Chun CL, Penn RL, Arnold WA (2006) Kinetic and microscopic studies of reductive transformations of organic

contaminants on goethite. Environ Sci Technol 40(10):3299–3304. https://doi.org/10.1021/es0600983
Cooper DC, Picardal F, Rivera J, Talbot C (2000) Zinc immobilization and magnetite formation via ferric oxide reduction by *Shewanella putrefaciens* 200. Environ Sci Technol 34(1):100–106. https://doi.org/10.1021/es990510x
Cooper DC, Picardal FF, Coby AJ (2006) Interactions between microbial iron reduction and metal geochemistry: effect of redox cycling on transition metal speciation in iron bearing sediments. Environ Sci Technol 40(6):1884–1891. https://doi.org/10.1021/es051778t
Cornell RM, Schwertmann U (2004) The iron oxides: structure, properties, reactions, occurences and uses, 2nd edn. Wiley
Coward EK, Ohno T, Plante AF (2018) Adsorption and molecular fractionation of dissolved organic matter on iron-bearing mineral matrices of varying crystallinity. Environ Sci Technol 52(3):1036–1044. https://doi.org/10.1021/acs.est.7b04953
Crosby HA, Johnson CM, Roden EE, Beard BL (2005) Coupled Fe(II)–Fe(III) electron and atom exchange as a mechanism for Fe isotope fractionation during dissimilatory iron oxide reduction. Environ Sci Technol 39(17):6698–6704. https://doi.org/10.1021/es0505346
Curti E, Fujiwara K, Iijima K, Tits J, Cuesta C, Kitamura A, Glaus MA, Müller W (2010) Radium uptake during barite recrystallization at 23 ± 2 °C as a function of solution composition: an experimental 133Ba and 226Ra tracer study. Geochim Cosmochim Acta 74(12):3553–3570. https://doi.org/10.1016/j.gca.2010.03.018
Das S, Hendry MJ, Essilfie-Dughan J (2011) Effects of adsorbed arsenate on the rate of transformation of 2-line ferrihydrite at pH 10. Environ Sci Technol 45(13):5557–5563. https://doi.org/10.1021/es200107m
Eglinton TI (2012) Geochemistry: a rusty carbon sink. Nature 483(7388):165–166. https://doi.org/10.1038/483165a
Ekstrom EB, Learman DR, Madden AS, Hansel CM (2010) Contrasting effects of Al substitution on microbial reduction of Fe(III) (hydr)oxides. Geochim Cosmochim Acta 74(24):7086–7099. https://doi.org/10.1016/j.gca.2010.09.008
Eusterhues K, Wagner FE, Haeusler W, Hanzlik M, Knicker H, Totsche KU, Koegel-Knabner I, Schwertmann U (2008) Characterization of ferrihydrite-soil organic matter coprecipitates by X-ray diffraction and Mssbauer spectroscopy. Environ Sci Technol 42(21):7891–7897
Felmy AR, Ilton ES, Rosso KM, Zachara JM (2011) Interfacial reactivity of radionuclides: emerging paradigms from molecular-level observations. Mineral Mag 75(4):2379–2391. https://doi.org/10.1180/minmag.2011.075.4.2379
Flynn ED, Catalano JG (2018) Influence of oxalate on Ni fate during Fe(II)-catalyzed recrystallization of hematite and goethite. Environ Sci Technol 52(12):6920–6927. https://doi.org/10.1021/acs.est.8b00641
Fredrickson JK, Zachara JM, Kennedy DW, Dong HL, Onstott TC, Hinman NW, Li SM (1998) Biogenic iron mineralization accompanying the dissimilatory reduction of hydrous ferric oxide by a groundwater bacterium. Geochim Cosmochim Acta 62(19–20):3239–3257. https://doi.org/10.1016/S0016-7037(98)00243-9
Fredrickson JK, Kota S, Kukkadapu RK, Liu CX, Zachara JM (2003) Influence of electron donor/acceptor concentrations on hydrous ferric oxide (HFO) bioreduction. Biodegradation 14(2):91–103. https://doi.org/10.1023/a:1024001207574
Frierdich AJ, Catalano JG (2012) Controls on Fe(II)-activated trace element release from goethite and hematite. Environ Sci Technol 46(3):1519–1526. https://doi.org/10.1021/es203272z
Frierdich AJ, Scherer MM, Bachman JE, Engelhard MH, Rapponotti BW, Catalano JG (2012) Inhibition of trace element release during Fe(II)-activated recrystallization of Al-, Cr-, and Sn-substituted goethite and hematite. Environ Sci Technol 46(18):10031–10039. https://doi.org/10.1021/es302137d
Frierdich AJ, Beard BL, Reddy TR, Scherer MM, Johnson CM (2014a) Iron isotope fractionation between aqueous Fe(II) and goethite revisited: new insights based on a multi-direction approach to equilibrium and isotopic exchange rate modification. Geochim Cosmochim Acta 139:383–398. https://doi.org/10.1016/j.gca.2014.05.001
Frierdich AJ, Beard BL, Scherer MM, Johnson CM (2014b) Determination of the Fe(II)aq–magnetite equilibrium iron isotope fractionation factor using the three-isotope method and a multi-direction approach to equilibrium. Earth Planet Sci Lett 391:77–86. https://doi.org/10.1016/j.epsl.2014.01.032
Frierdich AJ, Beard BL, Rosso KM, Scherer MM, Spicuzza MJ, Valley JW, Johnson CM (2015a) Low temperature, non-stoichiometric oxygen-isotope exchange coupled to Fe(II)–goethite interactions. Geochim Cosmochim Acta 160:38–54. https://doi.org/10.1016/j.gca.2015.03.029
Frierdich AJ, Helgeson M, Liu C, Wang C, Rosso KM, Scherer MM (2015b) Iron atom exchange between hematite and aqueous Fe(II). Environ Sci Technol 49(14):8479–8486. https://doi.org/10.1021/acs.est.5b01276
Frierdich AJ, Nebel O, Beard BL, Johnson CM (2019a) Iron isotope exchange and fractionation between hematite ($\alpha$-$Fe_2O_3$) and aqueous Fe(II): a combined three-isotope and reversal-approach to equilibrium study. Geochim Cosmochim Acta 245(15):207–221. https://doi.org/10.1016/j.gca.2018.10.033
Frierdich AJ, Saxey DW, Adineh VR, Fougerouse D, Reddy SM, Rickard WD, Sadek AZ, Southall SC (2019b) Direct observation of nanoparticulate goethite recrystallization by atom probe analysis of isotopic tracers. Environ Sci Technol 53(22):13126–13135. https://doi.org/10.1021/acs.est.9b04191
Gaboriaud F, Ehrhardt J (2003) Effects of different crystal faces on the surface charge of colloidal goethite (alpha-FeOOH) particles: an experimental and modeling study. Geochim Cosmochim Acta 67(5):967–983. https://doi.org/10.1016/s0016-7037(02)00988-2
Gault B, Moody MP, Geuser FD, Tsafnat G, Fontaine AL, Stephenson LT, Haley D, Ringer SP (2009) Advances in the calibration of atom probe tomographic reconstruction. J Appl Phys 105(3):618
Gorski CA, Fantle MS (2017) Stable mineral recrystallization in low temperature aqueous systems: a critical review.

Geochim Cosmochim Acta 198:439–465. https://doi.org/10.1016/j.gca.2016.11.013

Gorski CA, Handler RM, Beard BL, Pasakarnis T, Johnson CM, Scherer MM (2012) Fe atom exchange between aqueous Fe(2+) and magnetite. Environ Sci Technol 46(22):12399–12407. https://doi.org/10.1021/es204649a

Gorski CA, Edwards R, Sydney M, Hofstetter TB, Stewart SM (2016) Thermodynamic characterization of iron oxide-aqueous $Fe^{2+}$ redox couples. Environ Sci Technol 50(16):8538–8547. https://doi.org/10.1021/acs.est.6b02661

Guo HB, Xu HF, Barnard AS (2013) Can hematite nanoparticles be an environmental indicator? Energy Environ Sci 6(2):561–569. https://doi.org/10.1039/c2ee23253g

Handler RM, Beard BL, Johnson CM, Scherer MM (2009) Atom exchange between aqueous Fe(II) and goethite: an Fe isotope tracer study. Environ Sci Technol 43(4):1102–1107. https://doi.org/10.1021/es802402m

Handler RM, Frierdich AJ, Johnson CM, Rosso KM, Beard BL, Wang C, Latta DE, Neumann A, Pasakarnis T, Premaratne WA, Scherer MM (2014) Fe(II)-catalyzed recrystallization of goethite revisited. Environ Sci Technol 48(19):11302–11311. https://doi.org/10.1021/es503084u

Hansel CM, Benner SG, Neiss J, Dohnalkova A, Kukkadapu RK, Fendorf S (2003) Secondary mineralization pathways induced by dissimilatory iron reduction of ferrihydrite under advective flow. Geochim Cosmochim Acta 67(16):2977–2992. https://doi.org/10.1016/s0016-7037(03)00276-x

Hansel CM, Benner SG, Fendorf S (2005) Competing Fe (II)-induced mineralization pathways of ferrihydrite. Environ Sci Technol 39(18):7147–7153. https://doi.org/10.1021/es050666z

Hiemstra T, Riemsdijk WHV (1999) Effect of different crystal faces on experimental interaction force and aggregation of hematite. Langmuir 15(23):8045–8051. https://doi.org/10.1021/la9903604

Hiemstra T, Venema P, Riemsdijk WHV (1996) Intrinsic proton affinity of reactive surface groups of metal (hydr) oxides: the bond valence principle. J Colloid Interface Sci 184(2):680. https://doi.org/10.1006/jcis.1996.0666

Hren MT, Lowe DR, Tice MM, Byerly G, Chamberlain CP (2006) Stable isotope and rare earth element evidence for recent ironstone pods within the Archean Barberton greenstone belt, South Africa. Geochim Cosmochim Acta 70(6):1457–1470. https://doi.org/10.1016/j.gca.2005.11.016

Hu S, Liang Y, Liu T, Li F, Lu Y, Shi Z (2020) Kinetics of As(V) and carbon sequestration during Fe(II)-induced transformation of ferrihydrite-As(V)-fulvic acid coprecipitates. Geochim Cosmochim Acta 272:160–176. https://doi.org/10.1016/j.gca.2020.01.002

Hu S, Wu Y, Shi Z, Li F, Liu T (2021) Quinone-mediated dissimilatory iron reduction of hematite: interfacial reactions on exposed 001 and 100 facets. J Colloid Interface Sci 583:544–552. https://doi.org/10.1016/j.jcis.2020.09.074

Hua J, Fei Y, Feng C, Liu C, Liang S, Wang S-L, Wu F (2022a) Anoxic oxidation of As(III) during Fe(II)-induced goethite recrystallization: evidence and importance of Fe(IV) intermediate. J Hazard Mater. https://doi.org/10.1016/j.jhazmat.2021.126806

Huang X, Hou X, Zhang X, Rosso KM, Zhang L (2018) Facet-dependent contaminant removal properties of hematite nanocrystals and their environmental implications. Environ Sci Nano 5(8):1790–1806. https://doi.org/10.1039/c8en00548f

Huang J, Jones A, Waite TD, Chen Y, Huang X, Rosso KM, Kappler A, Mansor M, Tratnyek PG, Zhang H (2021) Fe(II) redox chemistry in the environment. Chem Rev 121(13):8161–8233. https://doi.org/10.1021/acs.chemrev.0c01286

Hug SJ, Leupin O (2003) Iron-catalyzed oxidation of arsenic(III) by oxygen and by hydrogen peroxide: pH-dependent formation of oxidants in the Fenton reaction. Environ Sci Technol 37(12):2734–2742. https://doi.org/10.1021/es026208x

Jakub Z, Meier M, Kraushofer F, Balajka J, Pavelec J, Schmid M, Franchini C, Diebold U, Parkinson GS (2021) Rapid oxygen exchange between hematite and water vapor. Nat Commun. https://doi.org/10.1038/s41467-021-26601-4

Jang JH, Dempsey BA, Catchen GL, Burgos WD (2003) Effects of Zn(II), Cu(II), Mn(II), Fe(II), $NO_3^-$, or $SO_4^{2-}$ at pH 6.5 and 8.5 on transformations of hydrous ferric oxide (HFO) as evidenced by Mössbauer spectroscopy. Colloid Surf A 221(1–3):55–68. https://doi.org/10.1016/S0927-7757(03)00134-1

Jones AM, Collins RN, Rose J, Waite TD (2009) The effect of silica and natural organic matter on the Fe(II)-catalysed transformation and reactivity of Fe(III) minerals. Geochim Cosmochim Acta 73(15):4409–4422. https://doi.org/10.1016/j.gca.2009.04.025

Jones AM, Collins RN, Waite TD (2017) Redox characterization of the Fe(II)-catalyzed transformation of ferrihydrite to goethite. Geochim Cosmochim Acta 218:257–272. https://doi.org/10.1016/j.gca.2017.09.024

Joshi P, Gorski CA (2016) Anisotropic morphological changes in goethite during Fe(2+)-catalyzed recrystallization. Environ Sci Technol 50(14):7315–7324. https://doi.org/10.1021/acs.est.6b00702

Joshi P, Fantle MS, Larese-Casanova P, Gorski CA (2017) Susceptibility of goethite to Fe2+-catalyzed recrystallization over time. Environ Sci Technol. https://doi.org/10.1021/acs.est.7b02603

Joshi P, Fantle MS, Boualavong J, Gorski CA (2022) Quantifying the rate of Fe2+-catalyzed recrystallization based on a unifying model framework. Geochim Cosmochim Ac. https://doi.org/10.1016/j.gca.2022.08.019

Kang K, Schenkeveld WD, Biswakarma J, Borowski SC, Hug SJ, Hering JG, Kraemer SM (2018) Low Fe(II) concentrations catalyze the dissolution of various Fe(III)(hydr) oxide minerals in the presence of diverse ligands and over a broad pH range. Environ Sci Technol 53(1):98–107. https://doi.org/10.1021/acs.est.8b03909

Karimian N, Johnston SG, Burton ED (2017) Antimony and arsenic behavior during Fe(II)-induced transformation of jarosite. Environ Sci Technol 51(8):4259–4268. https://doi.org/10.1021/acs.est.6b05335

Karimian N, Burton ED, Johnston SG (2019) Antimony speciation and mobility during Fe(II)-induced transformation

of humic acid-antimony(V)-iron(III) coprecipitates. Environ Pollut 254(Pt B):113112. https://doi.org/10.1016/j.envpol.2019.113112

Kerisit S, Zarzycki P, Rosso KM (2015) Computational molecular simulation of the oxidative adsorption of ferrous iron at the hematite (001)-water interface. J Phys Chem C 119(17):9242–9252. https://doi.org/10.1021/jp512422h

Kim SH, Lee JY, Ahn JP, Choi PP (2019) Fabrication of atom probe tomography specimens from nanoparticles using a fusible Bi–In–Sn alloy as an embedding medium. Microsc Microanal 25(3):438–446

Klausen J, Troeber SP, Haderlein SB, Schwarzenbach RP (1995) Reduction of substituted nitrobenzenes by Fe(II) in aqueous mineral suspensions. Environ Sci Technol 29(9):2396–2404. https://doi.org/10.1021/es00009a036

Lalonde K, Mucci A, Ouellet A, Gelinas Y (2012) Preservation of organic matter in sediments promoted by iron. Nature 483(7388):198–200. https://doi.org/10.1038/nature10855

Larese-Casanova P, Scherer MM (2007a) Fe(II) sorption on hematite: new insights based on spectroscopic measurements. Environ Sci Technol 41(2):471–477

Larese-Casanova P, Scherer MM (2007b) Morin transition suppression in Polycrystalline (57)Hematite (alpha-Fe2O3) exposed to Fe-56(II). Hyperfine Interact 174(1–3):111–119. https://doi.org/10.1007/s10751-007-9517-4

Larese-Casanova P, Kappler A, Haderlein SB (2012) Heterogeneous oxidation of Fe(II) on iron oxides in aqueous systems: Identification and controls of Fe(III) product formation. Geochim Cosmochim Acta 91:171–186. https://doi.org/10.1016/j.gca.2012.05.031

Latta DE, Bachman JE, Scherer MM (2012a) Fe electron transfer and atom exchange in goethite: influence of Al-substitution and anion sorption. Environ Sci Technol 46(19):10614–10623. https://doi.org/10.1021/es302094a

Latta DE, Gorski CA, Scherer MM (2012b) Influence of $Fe^{2+}$-catalysed iron oxide recrystallization on metal cycling. Biochem Soc Trans 40(6):1191–1197. https://doi.org/10.1042/BST20120161

Li XX, Sheng AX, Ding YF, Liu J (2022) A model towards understanding stabilities and crystallization pathways of iron (oxyhydr)oxides in redox-dynamic environments. Geochim Cosmochim Acta 336:92–103. https://doi.org/10.1016/j.gca.2022.09.002

Lies DP, Hernandez ME, Kappler A, Mielke RE, Gralnick JA, Newman DK (2005) Shewanella oneidensis MR-1 uses overlapping pathways for iron reduction at a distance and by direct contact under conditions relevant for biofilms. Appl Environ Microbiol 71(8):4414–4426. https://doi.org/10.1128/aem.71.8.4414-4426.2005

Liu H, Li P, Zhu M, Wei Y, Sun Y (2007) Fe(II)-induced transformation from ferrihydrite to lepidocrocite and goethite. J Solid State Chem 180(7):2121–2128. https://doi.org/10.1016/j.jssc.2007.03.022

Liu C, Zhu Z, Li F, Liu T, Liao C, Lee J-J, Shih K, Tao L, Wu Y (2016) Fe(II)-induced phase transformation of ferrihydrite: the inhibition effects and stabilization of divalent metal cations. Chem Geol 444:110–119. https://doi.org/10.1016/j.chemgeo.2016.10.002

Liu CS, Chen MJ, Li FB, Tao L, Xia YF (2019) Stabilization of $Cd^{2+}$/$Cr^{3+}$ during aqueous Fe(II)-induced recrystallization of Al-substituted goethite. Soil Sci Soc Am J 83(2):483–491

Liu J, Chen Q, Yang Y, Wei H, Laipan M, Zhu R, He H, Hochella MF Jr (2022) Coupled redox cycling of Fe and Mn in the environment: The complex interplay of solution species with Fe- and Mn-(oxyhydr)oxide crystallization and transformation. Earth-Sci Rev. https://doi.org/10.1016/j.earscirev.2022.104105

Lu Y, Hu S, Wang Z, Ding Y, Lu G, Lin Z, Dang Z, Shi Z (2019) Ferrihydrite transformation under the impact of humic acid and Pb: kinetics, nanoscale mechanisms, and implications for C and Pb dynamics. Environ Sci-Nano 6(3):747–762. https://doi.org/10.1039/c8en01327f

Lu Y, Hu SW, Liu F, Liang YZ, Shi ZQ (2020) Effects of humic acid and fulvic acid on the sequestration of copper and carbon during the iron oxide transformation. Chem Eng J. https://doi.org/10.1016/j.cej.2019.123194

Lv J, Miao Y, Huang Z, Hang R, Zhang S (2018) Facet-mediated adsorption and molecular fractionation of humic substances on hematite surfaces. Environ Sci Technol 52(22):13662–13662. https://doi.org/10.1021/acs.est.8b05875

Massey MS, Lezama-Pacheco JS, Michel FM, Fendorf S (2014) Uranium incorporation into aluminum-substituted ferrihydrite during iron(II)-induced transformation. Environ Sci Process Impacts 16(9):2137–2144. https://doi.org/10.1039/c4em00148f

McBriarty ME, Stubbs JE, Eng PJ, Rosso KM (2018) Potential-specific structure at the hematite-electrolyte interface. Adv Funct Mater. https://doi.org/10.1002/adfm.201705618

Melton ED, Swanner ED, Behrens S, Schmidt C, Kappler A (2014) The interplay of microbially mediated and abiotic reactions in the biogeochemical Fe cycle. Nat Rev Microbiol 12(12):797–808. https://doi.org/10.1038/nrmicro3347

Noor N, Thompson A (2022) Localized alteration of ferrihydrite natural organic matter coprecipitates following reaction with Fe(II). Soil Sci Soc Am J 86(2):253–263. https://doi.org/10.1002/saj2.20366

Notini L, Latta DE, Neumann A, Pearce CI, Sassi M, N'Diaye AT, Rosso KM, Scherer MM (2018) The role of defects in Fe (II)–goethite electron transfer. Environ Sci Technol 52(5):2751–2759. https://doi.org/10.1021/acs.est.7b05772

Notini L, Byrne JM, Tomaszewski EJ, Latta DE, Zhou Z, Scherer MM, Kappler A (2019a) Mineral defects enhance bioavailability of goethite toward microbial Fe(III) reduction. Environ Sci Technol 53(15):8883–8891. https://doi.org/10.1021/acs.est.9b03208

Notini L, Latta DE, Neumann A, Pearce CI, Schefer MM (2019b) A closer look at Fe(II) passivation of goethite. ACS Earth Space Chem 3(12):2717–2725. https://doi.org/10.1021/acsearthspacechem.9b00224

Notini L, ThomasArrigo LK, Kaegi R, Kretzschmar R (2022) Coexisting goethite promotes Fe(II)-catalyzed transformation of ferrihydrite to goethite. Environ Sci Technol. https://doi.org/10.1021/acs.est.2c03925

Pedersen HD, Postma D, Jakobsen R, Larsen O (2005) Fast transformation of iron oxyhydroxides by the catalytic action of aqueous Fe(II). Geochim Cosmochim Acta

69(16):3967–3977. https://doi.org/10.1016/j.gca.2005.03.016

Perez JPH, Tobler DJ, Thomas AN, Freeman HM, Dideriksen K, Radnik J Jr, Benning LG (2019) Adsorption and reduction of arsenate during the Fe2+-induced transformation of ferrihydrite. ACS Earth Space Chem 3(6):884–894. https://doi.org/10.1021/acsearthspacechem.9b00031

Pestovsky O, Bakac A (2004a) Reactivity of aqueous Fe(IV) in hydride and hydrogen atom transfer reactions. J Am Chem Soc 126(42):13757–13764. https://doi.org/10.1021/ja0457112

Piepenbrock A, Dippon U, Porsch K, Appel E, Kappler A (2011) Dependence of microbial magnetite formation on humic substance and ferrihydrite concentrations. Geochim Cosmochim Acta 75(22):6844–6858. https://doi.org/10.1016/j.gca.2011.09.007

Qiu G, Gao T, Hong J, Tan W, Liu F, Zheng L (2017) Mechanisms of arsenic-containing pyrite oxidation by aqueous arsenate under anoxic conditions. Geochim Cosmochim Acta 217:306–319. https://doi.org/10.1016/j.gca.2017.08.030

Reddy TR, Frierdich AJ, Beard BL, Johnson CM (2015) The effect of pH on stable iron isotope exchange and fractionation between aqueous Fe(II) and goethite. Chem Geol 397(18):118–127. https://doi.org/10.1016/j.chemgeo.2015.01.018

Redman AD, Macalady DL, Ahmann D (2002) Natural organic matter affects arsenic speciation and sorption onto hematite. Environ Sci Technol 36(13):2889–2896. https://doi.org/10.1021/es0112801

Rosso KM, Yanina SV, Gorski CA, Laresecasanova P, Scherer MM (2010) Connecting observations of hematite (alpha-$Fe_2O_3$) growth catalyzed by Fe(II). Environ Sci Technol 44(1):61–67. https://doi.org/10.1021/es901882a

Russell B, Payne M, Ciacchi LC (2009) Density functional theory study of Fe(II) adsorption and oxidation on goethite surfaces. Phys Rev B. https://doi.org/10.1103/PhysRevB.79.165101

Schwertmann U (1983) Effect of pH on the formation of goethite and hematite from ferrihydrite. Clays Clay Miner 31(4):277–284. https://doi.org/10.1346/CCMN.1983.0310405

Schwertmann U, Carlson L, Fechter H (1984) Iron oxide formation in artificial ground waters. Schwzerische Ztschrift Für Hydrologie 46(2):185–191. https://doi.org/10.1007/BF02538060

Schwertmann U, Stanjek H, Becher HH (2004) Long-term in vitro transformation of 2-line ferrihydrite to goethite/hematite at 4, 10, 15 and 25 degrees C. Clay Miner 39(4):433–438. https://doi.org/10.1180/0009855043940145

Schwertmann U, Wagner F, Knicker H (2005) Ferrihydrite-humic associations: magnetic hyperfine interactions. Soil Sci Soc Am J 69(4):1009–1015. https://doi.org/10.2136/sssaj2004.0274

Sheng AX, Li XX, Arai YJ, Ding YF, Liu J (2020a) Citrate controls Fe(II)-catalyzed transformation of ferrihydrite by complexation of the labile Fe(III) intermediate. Environ Sci Technol 54(12):7309–7319. https://doi.org/10.1021/acs.est.0c00996

Sheng AX, Liu J, Li XX, Qafoku O, Collins RN, Jones AM, Pearce CI, Cm W, Ni JR, Lu Ah (2020b) Labile Fe(III) from sorbed Fe(II) oxidation is the key intermediate in Fe(II)-catalyzed ferrihydrite transformation. Geochim Cosmochim Acta 272(1):105–120. https://doi.org/10.1016/j.gca.2019.12.028

Sheng A, Liu J, Li X, Luo L, Ding Y, Chen C, Zhang X, Wang C, Rosso KM (2021) Labile Fe(III) supersaturation controls nucleation and properties of product phases from Fe(II)-catalyzed ferrihydrite transformation. Geochim Cosmochim Acta 309:272–285. https://doi.org/10.1016/j.gca.2021.06.027

Shu Z, Liu L, Tan W, Suib SL, Qiu G, Yang X, Zheng L, Liu F (2019) Solar irradiation induced transformation of ferrihydrite in the presence of aqueous Fe(II). Environ Sci Technol 53(15):8854–8861. https://doi.org/10.1021/acs.est.9b02750

Southall SC, Micklethwaite S, Wilson SA, Frierdich AJ (2018) Changes in crystallinity and tracer-isotope distribution of goethite during Fe(II)-accelerated recrystallization. ACS Earth Space Chem 2(12):1271–1282. https://doi.org/10.1021/acsearthspacechem.8b00100

Stumm W, Sulzberger B (1992) The cycling of iron in natural environments: considerations based on laboratory studies of heterogeneous redox processes. Geochim Cosmochim Acta 56(8):3233–3257. https://doi.org/10.1016/0016-7037(92)90301-X

Su XW, Liu J (2019) Highlights and breakthroughs iron carbide in the core. Am Mineral 104(1):1–1. https://doi.org/10.2138/am-2019-6835

Sun J, Chillrud SN, Mailloux BJ, Bostick BC (2016a) In situ magnetite formation and long-term arsenic immobilization under advective flow conditions. Environ Sci Technol 50(18):10162–10171. https://doi.org/10.1021/acs.est.6b02362

Sun J, Chillrud SN, Mailloux BJ, Stute M, Singh R, Dong H, Lepre CJ, Bostick BC (2016b) Enhanced and stabilized arsenic retention in microcosms through the microbial oxidation of ferrous iron by nitrate. Chemosphere 144:1106–1115. https://doi.org/10.1016/j.chemosphere.2015.09.045

Sun J, Mailloux BJ, Chillrud SN, van Geen A, Thompson A, Bostick BC (2018) Simultaneously quantifying ferrihydrite and goethite in natural sediments using the method of standard additions with X-ray absorption spectroscopy. Chem Geol 476:248–259. https://doi.org/10.1016/j.chemgeo.2017.11.021

Taylor SD, Liu J, Arey BW, Schreiber DK, Perea DE, Rosso KM (2018) Resolving iron(II) sorption and oxidative growth on hematite (001) using atom probe tomography. J Phys Chem C 122(7):3903–3914. https://doi.org/10.1021/acs.jpcc.7b11989

Taylor SD, Kovarik L, Cliff JB, Rosso KM (2019a) Facet-selective adsorption of Fe(II) on hematite visualized by nanoscale secondary ion mass spectrometry. Environ Sci-Nano. https://doi.org/10.1039/c9en00562e

Taylor SD, Liu J, Zhang X, Arey BW, Kovarik L, Schreiber DK, Perea DE, Rosso KM (2019b) Visualizing the iron atom exchange front in the Fe(II)-catalyzed recrystallization of goethite by atom probe tomography. Proc Natl

Acad Sci 116(8):2866–2874. https://doi.org/10.1073/pnas.1816620116

Teja AS, Koh PY (2009) Synthesis, properties, and applications of magnetic iron oxide nanoparticles. Prog Cryst Growth Charact Mater 55(1–2):22–45. https://doi.org/10.1016/j.pcrysgrow.2008.08.003

Tessier A, Fortin D, Belzile N, DeVitre RR, Leppard GG (1996) Metal sorption to diagenetic iron and manganese oxyhydroxides and associated organic matter: narrowing the gap between field and laboratory measurements. Geochim Cosmochim Acta 60(3):387–404. https://doi.org/10.1016/0016-7037(95)00413-0

Thamdrup B (2000) Bacterial manganese and iron reduction in aquatic sediments. In: Schink B (ed) Advances in microbial ecology, vol 16. Springer, Boston, pp 41–84

ThomasArrigo LK, Mikutta C, Byrne J, Kappler A, Kretzschmar R (2017) Iron(II)-catalyzed iron atom exchange and mineralogical changes in iron-rich organic freshwater flocs: an iron isotope tracer study. Environ Sci Technol 51(12):6897–6907. https://doi.org/10.1021/acs.est.7b01495

ThomasArrigo LK, Byrne JM, Kappler A, Kretzschmar R (2018) Impact of organic matter on iron(II)-catalyzed mineral transformations in ferrihydrite–organic matter coprecipitates. Environ Sci Technol 52(21):12316–12326. https://doi.org/10.1021/acs.est.8b03206

Tishchenko V, Meile C, Scherer MM, Pasakarnis TS, Thompson A (2015) Fe2+ catalyzed iron atom exchange and re-crystallization in a tropical soil. Geochim Cosmochim Acta 148:191–202. https://doi.org/10.1016/j.gca.2014.09.018

Wang L, Giammar DE (2015) Effects of pH, dissolved oxygen, and aqueous ferrous iron on the adsorption of arsenic to lepidocrocite. J Colloid Interface Sci 448:331–338. https://doi.org/10.1016/j.jcis.2015.02.047

Wang GF, Ran LY, Xu J, Wang YY, Ma LY, Zhu RL, Wei JM, He HP, Xi YF, Zhu JX (2021) Technical development of characterization methods provides insights into clay mineral-water interactions: a comprehensive review. Appl Clay Sci. https://doi.org/10.1016/j.clay.2021.106088

Weber KA, Achenbach LA, Coates JA (2006a) Microorganisms pumping iron: anaerobic microbial iron oxidation and reduction. Nat Rev Microbiol 4(10):752–764. https://doi.org/10.1038/nrmicro1490

Weber KA, Urrutia MM, Churchill PF, Kukkadapu RK, Roden EE (2006b) Anaerobic redox cycling of iron by freshwater sediment microorganisms. Environ Microbiol 8(1):100–113. https://doi.org/10.1111/j.1462-2920.2005.00873.x

Weidler PG, Hug SJ, Wetche TP, Hiemstra T (1998) Determination of growth rates of (100) and (110) faces of synthetic goethite by scanning force microscopy. Geochim Cosmochim Acta 62(21–22):3407–3412. https://doi.org/10.1016/s0016-7037(98)00251-8

Williams AGB, Scherer MM (2004) Spectroscopic evidence for Fe(II)–Fe(III) electron transfer at the iron oxide-water interface. Environ Sci Technol 38(18):4782–4790. https://doi.org/10.1021/es049373g

Wu F, Hua J, Zhou J, Liu Y, Long S, Fei Y, Liu C (2021) Facet-specific reactivity of hematite nanocrystals during Fe (II)-catalyzed recrystallization. Chem Geol. https://doi.org/10.1016/j.chemgeo.2021.120460

Xiao W, Jones AM, Collins RN, Bligh MW, Waite TD (2017) Use of Fourier transform infrared spectroscopy to examine the Fe(II)-catalyzed transformation of ferrihydrite. Talanta 175:30–37. https://doi.org/10.1016/j.talanta.2017.07.018

Xiao W, Jones AM, Li X, Collins RN, Waite TD (2018) Effect of *Shewanella oneidensis* on the kinetics of Fe(II)-catalyzed transformation of ferrihydrite to crystalline iron oxides. Environ Sci Technol 52(1):114–123. https://doi.org/10.1021/acs.est.7b05098

Yanina SV, Rosso KM (2008) Linked reactivity at mineral–water interfaces through bulk crystal conduction. Science 320(5873):218–222. https://doi.org/10.1126/science.1154833

Yund RA, Tullis J (1991) Compositional changes of minerals associated with dynamic recrystallization. Contrib Mineral Petrol 108(3):346–355. https://doi.org/10.1007/bf00285942

Zachara JM, Kukkadapu RK, Fredrickson JK, Gorby YA, Smith SC (2002) Biomineralization of poorly crystalline Fe(III) oxides by dissimilatory metal reducing bacteria (DMRB). Geomicrobiol J 19(2):179–207. https://doi.org/10.1080/01490450252864271

Zarzycki P, Rosso KM (2018) Surface charge effects on Fe(II) sorption and oxidation at (110) goethite surfaces. J Phys Chem C 122(18):10059–10066. https://doi.org/10.1021/acs.jpcc.8b02099

Zarzycki P, Rosso KM (2019) Energetics and the role of defects in Fe(II)-catalyzed goethite recrystallization from molecular simulations. ACS Earth Space Chem 3(2):262–272. https://doi.org/10.1021/acsearthspacechem.8b00175

Zarzycki P, Kerisit S, Rosso KM (2015a) Molecular dynamics study of Fe(II) adsorption, electron exchange, and mobility at goethite (alpha-FeOOH) surfaces. J Phys Chem C 119(6):3111–3123. https://doi.org/10.1021/jp511086r

Zarzycki P, Smith DM, Rosso KM (2015c) Proton dynamics on goethite nanoparticles and coupling to electron transport. J Chem Theory Comput 11(4):1715–1724. https://doi.org/10.1021/ct500891a

Zhang GQ, Yuan ZD, Lei L, Lin JR, Wang X, Wang SF, Jia Y (2019a) Arsenic redistribution and transformation during Fe(II)-catalyzed recrystallization of As-adsorbed ferrihydrite under anaerobic conditions. Chem Geol 525(20):380–389. https://doi.org/10.1016/j.chemgeo.2019.08.002

Zhou Z, Latta DE, Noor N, Thompson A, Borch T, Scherer MM (2018) Fe(II)-catalyzed transformation of organic

matter–ferrihydrite coprecipitates: a closer look using Fe isotopes. Environl Sci Technol 52(19):11142–11150. https://doi.org/10.1021/acs.est.8b03407

Zinder B, Furrer G, Stumm W (1986) The coordination chemistry of weathering. 2. Dissolution of Fe(III) oxides. Geochim Cosmochim Acta 50(9):1861–1869. https://doi.org/10.1016/0016-7037(86)90244-9

Zong M, Zhang X, Wang Y, Huang X, Zhou J, Wang Z, De Yoreo JJ, Lu X, Rosso KM (2019) Synthesis of 2D hexagonal hematite nanosheets and the crystal growth mechanism. Inorg Chem 58(24):16727–16735. https://doi.org/10.1021/acs.inorgchem.9b02883